Measurement Report: Investigation on the sources and formation processes of dicarboxylic acids and related species in urban aerosols before and during the COVID-19 lockdown in Jinan, East China

Jingjing Meng[1,2], Yachen Wang[1], Yuanyuan Li[1], Tonglin Huang[1], Zhifei Wang[3], Yiqiu, Wang[4], Min Chen[1], Zhanfang Hou[1], Houhua Zhou[5], Keding Lu[5], Kimitaka Kawamura[6], Pingqing Fu[2]

[1] School of Geography and Environment, Liaocheng University, Liaocheng 252000, China
[2] Institute of Surface-Earth System Science, School of Earth System Science, Tianjin University, Tianjin 300072, China
[3] Jinan Environmental Monitoring Center of Shandong Province, Jinan 250101, China
[4] Liaocheng Environmental Information and Monitoring Center, Liaocheng, 252000, China
[5] State Key Joint Laboratory of Environmental Simulation and Pollution Control, College of Environmental Sciences and Engineering, Peking University, Beijing 100871, China
[6] Chubu Institute for Advanced Studies, Chubu University, Kasugai 487-8501, Japan

Correspondence to: Pingqing Fu (fupingqing@tju.edu.cn)

Abstract. Dicarboxylic acid (Diacid) homologues are essential indicators of secondary organic aerosols (SOA) that exert considerable influence on climate changes and atmospheric chemistry. However, their sources and formation processes are poorly understood, leading to uncertainty in predicting the climate effect of SOA. A substantial drop in anthropogenic emissions during the COVID-19 lockdown (LCD) provides a "controlled experiment" to explore the effects of LCD measures and meteorological conditions on SOA. Here we investigated the difference in molecular distributions and stable carbon isotopic compositions ($\delta^{13}C$) of diacid homologues in $PM_{2.5}$ before and during the LCD. We found that the concentration and contribution of diacid homologues during the LCD were higher than before the LCD, indicating that the enhanced secondary oxidation could offset the reduction of anthropogenic emissions during the LCD. Higher oxalic acid (C_2)/diacids ratio and more positive $\delta^{13}C$ values of major diacids during the LCD suggested more aged organic aerosols. The enhanced C_2 and related species during the LCD were mainly derived from the promoted gaseous photochemical oxidation by the higher oxidants and stronger solar radiation. However, C_2 and related species before the LCD were dominantly derived from the aqueous oxidation of α-dicarbonyls depending on relative humidity and liquid water content. The increased $\delta^{13}C$ values of C_2 and other major diacids along with the high ratios of C_2/glyoxal, C_2/methylglyoxal, and C_2/diacids confirmed an isotopic fractionation effect during the oxidation process of precursors. Our results indicate that atmospheric pollution treatment depends on a balanced strategy and coordinated effort to control multiple pollutants.

1 Introduction

Water-soluble organic compounds (WSOC), constituting a great proportion of atmospheric fine particles, have attracted growing attention for the adverse effects on haze formation and global climate change (Lv et al., 2022; Wang et al., 2016). Dicarboxylic acids (diacids) and their organic precursors such as oxocarboxylic acids (oxoacids) and α-dicarbonyls are ubiquitous in the atmosphere, accounting for 14% of WSOC in particulate matter of urban regions (Ho et al., 2007; Kawamura and Bikkina, 2016), and can be up to 52% in marine regions (Bikkina et al., 2015). Due to the high solubility and hygroscopicity, diacid homologues can not only modify the hygroscopic growth of aerosols, but also improve the cloud condensation nuclei (CCN) activation, thus they exert an important effect on radiative forcing of aerosols via scattering the solar radiation and cloud formation (Ding et al., 2021; Wang et al., 2015).

Diacids and related compounds can be emitted directly from biogenic sources (Rinaldi et al., 2011), vehicle exhausts (Kawamura and Kaplan, 1987), and combustions of biomass and fossil fuels (Cao et al., 2017; Narukawa et al., 1999), while their relative contribution to total aerosol mass is negligible (Shen et al., 2022; Wang et al., 2020a). A growing body of evidence from modeling studies, chamber experiments, and field measurements inside and outside clouds have highlighted that most of these water-soluble organic acids are predominantly generated from the photochemical oxidation of volatile organic compounds (VOCs) followed by partitioning into the aqueous phase in wet aerosols, fog, and cloud droplets (Carlton et al., 2007; Ervens et al., 2004, 2011; Fu et al., 2008; Lim et al., 2013; Shen et al., 2022; Wang et al., 2010). Therefore, diacid homologues have been regarded as essential indicators of SOA in the atmosphere, which have been increasingly used to trace the aging processes and assess the oxidative capacity of the atmosphere (Enami et al., 2015; Zhao et al., 2020).

As the most abundant diacid with the lowest molecular weight, oxalic acid (C_2) is an important end product of numerous formation pathways in the aerosols; thus its formation mechanism has attracted great attention in the last decade. The strong correlation of C_2 with SO_4^{2-} at different observation sites suggests that both species shared a common production pathway (i.e., in-cloud processing) (Ding et al., 2021; Jung et al., 2010; Shen et al., 2023; Yu et al., 2005). A modeling study by Warneck (2003) revealed that the in-cloud formation pathway of C_2 from the oxidation of olefins with OH · radicals is crucially mediated by glyoxylic acid (ωC_2). A field study in the marine atmosphere by Crahan (2004) further supported such a formation mechanism of C_2. However, Carlton et al. (2007) conducted chamber experiments and found that glyoxal (Gly) is oxidized by OH · radicals in aqueous phase to produce larger multifunctional compounds (not ωC_2) and ultimately degraded into C_2. This formation route of C_2 is different from the in-cloud processing. Furthermore, the C_2 formation via the ωC_2 pathway only accounts for less than 1% (Buxton et al., 1997; Calton et al., 2007). Perri et al. (2009) first confirmed that the oxidation of glycolaldehyde with OH ·radicals can not only produce C_2, glycolic acid, and ωC_2, but also form oligomer, malonic acid (C_3), and succinic acid (C_4). Many studies have demonstrated that C_2 is also derived from the photochemical breakdown/ decomposition of longer-chain diacids such as C_3 and C_4 (Kawamura and Usukura, 1993; Meng et al., 2021; Yu et al., 2021), but this process has been considered less important than the C_2 formation through the aqueous OH · radical oxidation (Carlton et al., 2007; Xu et al., 2022). Yu et al. (2019) reported that aqueous oxidation exerts a dominant effect on diacids and related compounds despite the increased contribution of photochemical oxidation in the gaseous phase during haze events in Beijing using multiple linear regression. A recent study by Xu et al. (2022) pointed out that a large portion of C_2 was derived from the aqueous process of organic precursors emitted from fossil fuel combustions. Laboratory simulation has demonstrated that C_2 can be oxidized by O_3 (Gligorovski et al., 2010), while field measurements have demonstrated that formation pathways influenced by O_3 are involved in the formation of C_2 (Meng et al., 2021; Mochizuki et al., 2017). The formation mechanism and influencing factors as well as the contribution of aqueous oxidation and gaseous photochemical oxidation are still not well understood. Therefore, further investigations on C_2 and related compounds are necessary to provide a knowledge base for a better understanding of SOA and improving the accuracy of the aerosol model.

To curb the transmission of the novel coronavirus disease 2019 (hereafter referred to as COVID-19) in human society, a strict lockdown (LCD) measure was first implemented by the Chinese government starting at the end of January 2020 (Le et al., 2020). These dramatic restrictions resulted in a sharp drop-off in air pollutants (Li et al., 2021a; Meng et al., 2021), for instance, the average concentrations of five parameters including CO, NO_2, SO_2, $PM_{2.5}$, and PM_{10} decreased by 4.6–24.7% in 44 cities of China because of the travel restrictions during the LCD (Bao and Zhang, 2020). Unexpectedly, a few haze episodes still occurred in China during the LCD. Online observations, model simulations, and satellite measurements have pointed out that the appearance of haze events during the LCD was mainly caused by the unfavorable meteorological conditions, continuous emissions of SO_2, NO_X, and VOCs from power plants and petrochemical refineries, and an enhanced SOA formation (Huang et al., 2020; Li et al., 2020; Wang et al., 2020b; Shi et al., 2021; Zhong et al., 2021). These studies focused on the effect of the LCD policies on air quality and haze formation, for example, Le et al. (2020) and Huang et al. (2020) pointed out that the reduction of NO_X emissions lead to the enhanced ozone concentration, further improved the atmospheric oxidizing capacity and promoted the formation of secondary aerosol during the LCD. However, little is known about the impact of LCD measures on the molecular distributions, aging processes, and the formation mechanisms of SOA from field observations.

In order to understand the effect of the reduced anthropogenic emissions during the LCD and different meteorological parameters on the evolutionary process of homologous diacids and to investigate the relative contribution of aqueous oxidation versus gas-phase photochemical oxidation to total diacid homologues, fine aerosol samples in urban the city of Jinan, East China on a day/night basis before and during the LCD were collected. In this study, we first compare the differences in the molecular distributions, stable carbon isotopic compositions, and formation processes of C_2 and the related SOA before and during the LCD. Then, we investigate the effect of meteorological parameters (e.g., RH, temperature, and solar radiation) and aerosol aqueous properties (e.g., liquid water content (LWC) of aerosol and particle acidity (pH_{is})) on their formation processes in the urban atmosphere. Our results provide evidence for making policy as part of a comprehensive and cooperative public health strategy to improve air quality in megacities of China and elsewhere undergoing severe atmospheric pollution.

2 Experimental methods

2.1 Aerosol sampling

Fine aerosol ($PM_{2.5}$) sampling was conducted on the rooftop of a six-story building (36.67 °N, 117.06 °E, approximately 20 m above ground) that was about 40 m away from the Jinan Environment Monitoring Center (one of the State Controlling Air Sampling Sites in Jinan). The sampling site is in the center of the city of Jinan, which is located in the midwestern part of Shandong Province, China (Fig. S1). The sampling site lies in a typical urban setting surrounded by heavy traffic roads, residential areas, and commercial centers. $PM_{2.5}$ samples were collected using prebaked (450 °C, 8 h) quartz fiber filters (8 in. × 10 in.) from 6 January to 17 February 2020. The provincial government first performed the preventive LCD starting on 24 January 2020; thus the whole sampling period was divided into two periods: (1) before the LCD from 6 to 23 January, (2) during the LCD from 31 January to 17 February. Each sample lasted for 12 h on a day/night basis using a high-volume air sampler (TISCH, USA) at an airflow rate of 1.013 m^3 min^{-1}. The daytime samples were collected from 8:00 to 20:00, while nighttime samples were collected from 20:00 to 8:00 the next day. The field blank was sampled to check whether or not the aerosol samples have been polluted during the operation process, including the placing and collecting processes of the filter, which takes about a few minutes. The operating procedure of collecting field blank samples for 10 min in this study is conventional and scientifically sound and was also confirmed in other studies (Qi et al., 2022; Yi et al., 2021). Therefore, field blank samples were also collected by mounting the blank filter onto the sampler for 10 min without turning on the sampler before, during, and after the sampling campaign, respectively. A total of 72 $PM_{2.5}$ samples (36 for daytime and 36

for nighttime) and 6 field blank samples were collected in the whole sampling period. After the collection, each filter was sealed in an aluminum foil bag and stored in a freezer (−20 ℃) for about 16 months prior to analysis. The concentrations of $PM_{2.5}$, PM_{10}, CO, SO_2, NO_2, and O_3, as well as meteorological parameters such as wind direction/speed, RH, temperature, and solar radiation were retrieved from the monitoring station in the Jinan Environment Monitoring Center (https://www.aqistudy.cn/). The detailed information on quality assurance/quality control (QA/QC) of online data was described in Text S4. The inlet height of the air quality monitoring station was approximately 20 m above the ground level.

2.2 Chemical Analysis

2.2.1 Determination of diacids and related compounds as well as levoglucosan

The quantitative method for analyzing diacids, oxoacids, and α-dicarbonyls in $PM_{2.5}$ has been described previously (Fu et al., 2013; Meng et al., 2020). Briefly, a quarter of the filter was extracted with 5 mL pure Milli-Q water under ultrasonication three times. The water extracts were concentrated to near dryness and then reacted with 14% BF_3/*n*-butanol at 100 ℃ for 1 hour. During this process, the carboxyl functional group was derivatized to butyl ester, and the aldehyde and keto groups were derivatized to dibutoxy acetal. After derivatization, *n*-hexane was added and washed with pure water three times. Finally, the hexane layer was determined by a gas chromatography-mass spectrometry (GC-MS) and quantitatively analyzed using a GC (Agilent 6980) coupled with an HP-5 column (0.2mm × 25m, 0.5 μm film thickness) and a flame ionization detector (FID). GC-MS was performed on a Hewlett-Packard model Agilent 7890A GC coupled to a Hewlett-Packard model Agilent 5975C mass selective detector (MSD). GC separation was equipped with a split/splitless injector and a fused silica capillary column (DB-5MS, 30 m × 0.25 mm i.d., 0.25 μm film thickness). The GC oven temperature was programmed from 50°C for 2 min to 120°C at a rate of 15°C min^{-1}, and then to 300°C at a rate of 5°C min^{-1} with a final hold at 300°C for 16 min. The mass spectrometer was operated on the electron impact (IE) mode at 70 eV and scanned from 50 to 650 Da. The same analytical method as described above was also applied for field blank filters. As described in previous studies, the recoveries of C_2 ranged from 70% to 83% and other target compounds were better than 80% (Ding et al., 2021; Kawamura et al., 2013; Kawamura and Yasui, 2005; Meng et al., 2020; Zhao et al., 2020). Recoveries of the target compounds in this study were 80% for C_2 and higher than 85% for other organic species. Therefore, the percent recoveries mentioned in this study were good enough for such analysis.

Additionally, another portion of each filter sample was extracted with a mixture of dichloromethane and methanol (2:1, *v/v*) under ultrasonication. After being derivatized with 60 μL mixture of N, O-bis-(trimethylsilyl) trifluoroacetamide (BSTFA) and pyridine (5:1, *v/v*) at 70°C for 3 h, the derivatized extracts were identified for levoglucosan using a GC-MS (Yi et al., 2021). The recovery rate of levoglucosan is higher than 95%. Compared with the ambient samples, the concentration of levoglucosan in the field blank samples was lower than 4%. The data of targeted organic species presented in this study were corrected for both recoveries and field blanks.

2.2.2 Stable carbon isotopic composition of diacids and related compounds

The stable carbon isotopic compositions ($\delta^{13}C$) of major diacids and related compounds were measured using the method reported elsewhere (Kawamura and Watanabe, 2004). Briefly, 2 μL internal standard (*n*-C_{13} alkane, -27.24 ‰) was spiked to the ester fraction, and the $\delta^{13}C$ values of the derivatized samples relative to Pee Dee Belemnite (PDB) were measured using a GC-isotope ratio MS (GC-IR-MS, Thermo Fisher, Delta V Advantage). GC was installed with a HP manual on-column injector and a capillary column (CIP-Sil 8CB, 60 m × 0.32 mm × 0.25 μm) was used with a column oven temperature programmed from 50 to 120°C at a rate of 30°C min^{-1} and then to 300°C at a rate of 6°C min^{-1}. Flow rate of carrier gas (He) was maintained at 1.7 mL min^{-1}. Each sample was measured twice or three times to check the analytical error of the $\delta^{13}C$ values, which were less than 0.2‰. The $\delta^{13}C$ values were then calculated for free organic acids using an isotope mass

balance equation based on the measured $\delta^{13}C$ values of derivatives and the derivatizing agent (BF_3/*n*-butanol), as detailed in Text S1 (Kawamura and Watanabe, 2004).

2.2.3 Elemental carbon (EC), organic carbon (OC), WSOC, and inorganic ions

EC and OC in the $PM_{2.5}$ samples were analyzed using a DRI Model 2015 Carbon Analyzer following the Interagency Monitoring of Protected Visual Environments (IMPROVE) thermal/optical reflectance (TOR) protocol (Chow et al., 2004). As for the measurement of inorganic ions and WSOC, an aliquot of each sample filter was extracted with 30 mL Milli-Q water using an ultrasonic bath three times and then filtered through PTFE filters to remove particles and filter debris. The water extract was then divided into two parts. One part was analyzed for inorganic ions using an ion chromatography (Dionex 600, USA), and the other part was used to determine WSOC using a Total Carbon Analyzer (TOC-L CPH, Shimadzu, Japan).

2.3 Calculation of aerosol liquid water content (LWC), particle in-situ pH (pH_{is}), and OH ·radicals

As for the calculation of aerosol LWC and pH_{is}, the ISORROPIA-II model that treated the Na^+ - NH_4^+ - K^+ - Ca^{2+} - Mg^{2+} - SO_4^{2-} - NO_3^- - Cl^- system was applied. The forward mode with a metastable state in the ISORROPIA model was adopted (Fountoukis and Nenes, 2007).

Because of its short lifetime, high reactivity, and low concentration, the concentration of OH ·radicals in the atmosphere is greatly difficult to measure. Therefore, we used the TUV model (5.3 version) to calculate the time series of photolysis frequencies of ozone ($J(O^1D)$) before and during the LCD in Jinan, and then multiplied it by a factor of 4×10^{11} to estimate the corresponding time series of OH ·radical concentration (molecules cm^{-3}), based on the approximate linear relationship of OH ·radical concentration to $J(O^1D$ (Lu et al., 2019).

3 Results and Discussion

3.1 Meteorological conditions and air pollutants before and during the LCD

Temporal variations in the concentrations of $PM_{2.5}$, PM_{10}, gaseous pollutants, major chemical components of $PM_{2.5}$, and meteorological parameters before and during the LCD are summarized in Table 1 and presented in Fig. 1. Both temperature and solar radiation exhibited a continuously increasing trend, whereas RH before the LCD was 1.4 times higher than that during the LCD. Wind speed (3.0 ± 0.7 m s^{-1}) before the LCD was smaller than that (3.7 ± 1.1 m s^{-1}) during the LCD (Table 1), suggesting that air pollution caused by emissions from the local and surrounding regions of Jinan before the LCD was greater than that during the LCD, which was supported by the results of backward trajectory and potential source contribution function (PSCF) analysis (Fig. S1).

The parameters of air quality including $PM_{2.5}$, PM_{10}, CO, SO_2, and NO_2 decreased by 39–62% during the LCD (Table 1, Fig. 1), suggesting that the air quality was better during the LCD because of the substantial reduction of anthropogenic emissions. The haze event is defined as the daily average concentration of $PM_{2.5}$ larger than the Grade II of the Chinese National Ambient Air Quality Standard (75 μg m^{-3}) (Huang et al., 2014; Li et al., 2021b). Thirteen haze days before the LCD and four haze days during the LCD were observed in Jinan, respectively. Additionally, solar radiation (255 ± 117 W m^{-2}) during the LCD was stronger than that (164 ± 70 W m^{-2}) before the LCD (Table 1). It could be concluded that the atmosphere was clearer during the LCD than before the LCD, albeit the occurrence of several haze days. Being opposite to the other five air-quality parameters, O_3 concentration (66 ± 21 μg m^{-3}) during the LCD increased by 2.3 times compared to that (29 ± 18 μg m^{-3}) before the LCD (Table 1). Wang et al. (2021) demonstrated that O_3 in Chinese megacities during the LCD is primarily produced from the NO_x-saturated regime, where the drop of NO_x can lead to the enhanced O_3 concentration (Liu

and Wang, 2020). Firstly, the significant drop of NO_2 during the LCD resulted in the reduction of NO concentration (Xu et al., 2020), and further weakened the efficient titration effect of O_3 (Levy et al., 2014). Secondly, the reduction of NO_2 during the LCD could reduce the concentration of NO_3^- and further reduce the CCN number concentrations and additional shortwave cooling (Zaveri et al., 2021), thereby resulting in the alleviating aerosol radiative effects (aerosol–photolysis interaction) caused by aerosol absorbing or scattering solar radiation (Wu et al., 2020), which in turn enhanced the photochemical formation of O_3 (Liu and Wang, 2020). Besides, O_3 exhibited a negative correlation with $PM_{2.5}$ mass concentration ($R^2 = 0.57$) during the LCD, due to the weakened aerosol radiative effect on the photochemical formation of O_3 (Wu et al., 2020) and the reduced precursors of O_3 (Li et al., 2019). The more favorable atmospheric conditions such as the higher temperature and stronger solar radiation during the LCD were beneficial for the generation and accumulation of O_3 (Li et al., 2019). Being consistent with the variation of O_3 concentration, OH · radicals during the LCD (1.4×10^7 cm^{-3}) was 1.4 times higher than that (9.7×10^6 cm^{-3}) before the LCD (Table 1), which was also observed in other studies (Gaubert et al., 2021; Kang et al., 2021). The reduced NO_x during the LCD could lead to higher OH · radicals, because less OH · radicals could be consumed with NO_2 to produce nitric acid (Gaubert et al., 2021). Additionally, the elevated O_3 concentration during the LCD could result in the enhanced OH · radicals, as OH · radicals is mainly derived from O_3 photolysis with water vapor in the atmosphere (Kang et al., 2021).

The decreased concentrations of EC, OC, and WSOC in $PM_{2.5}$ but the enhanced ratios of OC/EC and WSOC/OC during the LCD (Table 1, Fig. 1) indicated more SOA productions due to the stronger photochemical oxidation during the LCD (Zhong et al., 2021). As a key tracer for biomass burning, levoglucosan showed a positive relationship with OC, EC, and WSOC ($R^2 \geq 0.45$) before the LCD rather than during the LCD ($R^2 \leq 0.15$) (Table S1), suggesting that biomass burning played an important role in carbonaceous species before the LCD rather than during the LCD. Secondary inorganic ions (SIA, the total concentration of SO_4^{2-}, NO_3^-, and NH_4^+) were dominant components of $PM_{2.5}$, which accounted for the higher percentages (47 ± 8%) in $PM_{2.5}$ mass during the LCD than that (40 ± 6%) before the LCD, indicating an enhanced formation of secondary aerosols during the LCD. The results of backward trajectory analysis showed that air masses before and during the LCD in Jinan were different (Fig. S1). Thus, the differences in the above chemical species and ratios may be not only because of different emission strengths and types of sources, but also due to different air masses between these two periods. The LWC concentration of aerosol is determined by RH and SIA concentration (Meng et al., 2020). Given the higher RH and SIA concentration before the LCD, the LWC concentration (35 ± 33 μg m^{-3}) before the LCD was 3.4 times higher than that (10 ± 10 μg m^{-3}) during the LCD. However, pH_{is} remained similar before (3.2 ± 3.0) and during the LCD (3.5 ± 3.5) with no significant statistical difference ($p > 0.05$, Table S2), indicating an insignificant difference in atmospheric aerosol acidity before and during the LCD.

3.2 Comparison of molecular distributions of diacids and related species before and during the LCD

A homogeneous series of diacids (C_2–C_{11}), oxoacids, and α-dicarbonyls identified in $PM_{2.5}$ samples before and during the LCD are summarized in Table 2. To avoid the effect of atmospheric dilution due to the variations of boundary layer height, we use the ratios of SOA species to EC or CO to explore the secondary production of organic species (Yu et al., 2021). As shown in Fig. 2, the ratio of total concentration of detected organic components (TDOCs) normalized by CO (TDOCs/CO) increased exponentially with the increase of temperature before ($y = 257.46e^{0.019x}$, $R^2 = 0.56$, Fig. 5a) and during ($y = 301.49e^{0.067x}$, $R^2 = 0.58$, Fig. 5c) the LCD, which was consistent with the Arrhenius Law, confirming that TDCOCs in this study were primarily derived from secondary formation and the contribution of primary emissions was insignificant. TDOCs are considered the stable products of secondary oxidation for a number of hydrocarbons (Martinelango et al., 2007). The loss of diacids (e.g., C_2) through the photolysis of iron oxalate complexes is a dominant sink from field observations and model studies (Cheng et al., 2017; Pavuluri and Kawamura, 2012; Weller et al., 2014; Zhou et al., 2015), while these species are more stable in the absence of Fe (Kunwar et al., 2019). Previous studies have pointed out that diacids and related compounds

presented a strong correlation with temperature, emphasizing the significance of secondary formation of those compounds with the increase in temperature (Kawamura and Bikkina, 2016; Kawamura and Yasui, 2005; Meng et al., 2014, 2018). Therefore, the loss of diacids and related compounds may be negligible when temperature increases. Additionally, the exponent(0.067) of the regression trend line during the LCD was 3.5 times higher ($p < 0.05$) than that (0.019) before the LCD, indicating that the oxidation rate during the LCD was larger. Different secondary formation rates of TDOCs between these two observation periods were possibly due to different meteorological factors (e.g., temperature, solar radiation, and RH), oxidants (e.g., O_3 and OH ·radical), emission strengths and types of organic precursors, physicochemical properties of aerosols (e.g., pH_{is} and LWC), and other influencing factors.

To verify if the concentrations of target compounds and major ratios were of significant difference, statistic tests were performed for $PM_{2.5}$ samples before and during the LCD (Table S2 and Table S3). As shown in Table S2, the concentrations of organic species (except for α-dicarbonyls) and major ratios in $PM_{2.5}$ before and during the LCD presented *p* values less than 0.05, indicating that the abundances and compositions of the major species before and during the LCD were statistically different. TDOCs exhibited an upward trend from 437 ± 117 ng m^{-3} (246 – 833 ng m^{-3}) before the LCD to 486 ± 144 ng m^{-3} (179 –825 ng m^{-3}) during the LCD (Table 2). The concentrations of diacids and oxoacids during the LCD increased by 1.1 and 2.1 times, respectively, while α-dicarbonyls during the LCD was almost the same as before the LCD. The concentrations of diacids and TDOCs reported in this study were significantly lower than those in Xi'an (Cheng et al., 2013), Chengdu (Li et al., 2015), Tianjin (Devineni et al., 2023; Zhao et al., 2023), Liaocheng (Meng et al., 2020), 14 Chinese cities, and other Asian megacities such as Padori, Daejeon (Zhao et al., 2023), Ulaanbaatar (Jung et al., 2010), Chennai (Pavuluri et al., 2010), and Tokyo (Kawamura and Yasui, 2005), but similar to those in Beijing (Zhao et al., 2018) and Guangzhou (Ho et al., 2011) during the wintertime (Table S4).

The daytime concentration of diacids before the LCD was 17% lower than that at night, which was opposite to the diurnal variation of diacids concentration during the LCD (Fig. 3a). As the predominant species throughout the whole observation period, C_2 concentration increased from 181 ± 47 ng m^{-3} before the LCD to 239 ± 108 ng m^{-3} during the LCD (Table 2), despite of the significant decrease in the primary pollutants from anthropogenic emissions during the LCD. C_2 is an end product derived from the photochemical decomposition of longer-chain diacids or secondary oxidation of α-dicarbonyls and oxoacids, thus the ratios of C_2/diacids and C_2/TDOCs can be considered essential tracers of aerosol aging (Wang et al., 2012; Zhao et al., 2020). Both ratios of C_2/diacids and C_2/TDOCs during the LCD were higher than those before the LCD (Fig. 3b), reflecting the presence of more aged organic aerosols during the LCD, which will be given more evidence in Section 3.5. Therefore, the concentration of C_2 as well as its relative abundance in total diacids and TDOCs were higher during the LCD than before the LCD, mainly due to the accelerated formation of C_2 during the LCD, which could offset the drop of organic precursors from anthropogenic emissions (Huang et al., 2020). Moreover, the daytime concentration of C_2 and the ratios of C_2/TDOCs and C_2/diacids were lower than those at night before the LCD but the opposite trends were found during the LCD, being consistent with the diurnal changes of total diacids before and during the LCD (Fig. 3). The second most abundant diacid was C_4, followed by C_3 and azelaic acid (C_9) before the LCD, while the second dominant diacid during the LCD was C_3, followed by C_4 and phthalic acid (Ph) (Table 2). Our results suggest that these species had different sources and underwent different formation processes because of different concentration levels of organic precursors and meteorological conditions before and during the LCD. Both ratios of C_2/C_4 and C_3/C_4 have been used as indicators of the photochemical aging of diacids, because the photochemical degradation of C_4 can lead to C_3, and C_3 can be photochemically oxidized into C_2 via intermediates (e.g., ketomalonic (kC_3) and hydroxymalonic acids) (Kawamura and Bikkina, 2016; Wang et al., 2010). Both C_2/C_4 (8.4 ± 3.4) and C_3/C_4 (1.6 ± 0.4) ratios during the LCD were higher than those (3.9 ± 1.5, 0.3 ± 0.1) before the LCD (Fig. 3b), indicating the stronger photochemical transformation of organic aerosols during the LCD. The C_3/C_4 ratio before the LCD was lower than that in other Asian megacities such as 14 Chinese cities (Ho et al., 2007), Beijing (Zhao et al., 2018), Daejeon (Devineni et al., 2023), and Chennai (Pavuluri et al., 2010), but comparable to that in Tianjin where biomass

burning, biogenic sources, and their aging contributed significantly to diacids and related compounds (Devineni et al., 2023) (Table S4). However, the C_3/C_4 ratio during the LCD was much higher than that in other Asian megacities (Table S4), again implying the significantly enhanced photochemical oxidation during the LCD. Previous studies have demonstrated that the C_3/C_4 ratio presented a strong correlation with temperature when the contribution of local sources predominates over long-distance transport (Kawamura and Usukura, 1993; Pavuluri et al., 2010a; Wang et al., 2020). In this study, the C_3/C_4 ratio was correlated strongly with temperature before the LCD ($R^2 = 0.54$, Fig. 4a), indicating that diacids before the LCD were largely influenced by local sources. However, the C_3/C_4 ratio was correlated moderately with temperature ($R^2 = 0.33$, Fig. 4b) during the LCD, suggesting that the contribution of local sources was equal to that of long-range transport to diacids during the LCD. These results were consistent with the results of backward trajectory and PSCF analysis (Fig. S1). The higher ratios of C_2/C_4 and C_3/C_4 during the LCD may be due to the local photooxidation and aging effects of long-distance transport.

Azelaic acid (C_9) is primarily derived from the secondary oxidation of unsaturated fatty acids (e.g., oleic acid) with a double bond at the C-9 position (Kawamura and Usukura, 1993), which is abundant in the fresh and aged aerosols emitted from biomass burning (Shen et al., 2022). It is noteworthy that the C_9 concentration (12 ± 4.0) before the LCD was 2.0 times higher than that (5.9 ± 4.8) during the LCD (Table 2), consistent with the variation of levoglucosan concentration (Table 1). C_9 showed a more robust relationship with levoglucosan before the LCD ($R^2 = 0.74$) than that ($R^2 = 0.06$) during the LCD (Table S1), suggesting that biomass burning was an essential contributor to C_9 before the LCD rather than during the LCD. Ph is primarily derived from the photochemical degradation of aromatic hydrocarbons (e.g., naphthalene) emitted from anthropogenic sources (Kawamura and Usukura, 1993). Although Ph was the most abundant diacid except for $C_2 - C_4$ during the LCD, its concentration (8.8 ± 6.1 ng m^{-3}) and relative abundance ($2.3 \pm 2.2\%$) in total diacids during the LCD were lower than those (11.0 ± 6.1 ng m^{-3}, $3.2 \pm 1.5\%$) before the LCD (Table 2, Fig. 3), suggesting the remarkable drop of anthropogenic emissions during the LCD.

As the important intermediate compounds of mono-carboxylic acids, oxoacids can ultimately generate diacids through aqueous oxidation (Carlton et al., 2007; Ervens et al., 2004). The diurnal variations of oxoacids presented similar patterns with diacids in each period (Fig. 3a). Moreover, oxoacids were correlated well with total diacids in each period, respectively ($R^2 > 0.5$, Fig. 2), indicating that oxoacids are the important intermediate species of diacids. The molecular distributions of oxoacids were characterized by the predominance ofωC_2 and pyruvic acid (Pyr) in each period. Previous studies have demonstrated that C_2 in urban aerosols is mainly generated from ωC_2 via aqueous oxidation (Cheng et al., 2015; Zhao et al., 2018). Therefore, C_2 was positively correlated with ωC_2 before and during the LCD, respectively ($R^2 > 0.5$, Fig. 4).

As the two smallest molecular weight α-dicarbonyls in the aerosols, glyoxal (Gly) and methylglyoxal (mGly) are originated from the photochemical oxidation of volatile organic compounds such as aromatics, isoprene, and monoterpenes in the gaseous phase, which are then partitioned into the aqueous phase of aerosols, and ultimately are oxidized to relatively lower volatility organic acids (e.g., ωC_2, Pyr, and C_2) (Carlton et al., 2007; Fu et al., 2008). Although the anthropogenic source emissions of α-dicarbonyls decreased dramatically during the LCD, the higher temperature and O_3 concentration during the LCD provided a favorable condition for α-dicarbonyls productions via secondary oxidation, which could offset the drop of primary emissions. Therefore, the concentration (24.7 ± 10.0 ng m^{-3}) of α-dicarbonyls during the LCD was about equal to that (25.1 ± 13.5 ng m^{-3}) before the LCD. Such differences in the molecular characteristics and aging level of diacids and related compounds before and during the LCD indicate substantially different formation pathways and influencing factors during these two observation periods, which will be discussed in more detail in Sections 3.3 and 3.4.

3.3 The aqueous-phase formation of diacids and related species before the LCD

As discussed above, the nighttime concentrations of C_2, diacids, and TDOCs exhibited higher values than those during the daytime. Such diurnal variations may be ascribed to the descended planetary boundary layer (PBL) height at night, which

can cause the enhanced concentrations of C_2 and related SOA. However, the increase in the ratios of C_2/diacids and C_2/TDOCs at night indicated that the effect of lowered nighttime PBL height was minor, which could be supported by the insignificant diurnal differences of primary pollutant markers such as Na^+, Ca^{2+}, and Mg^{2+} ($p > 0.05$, Table S3) between the daytime and nighttime. Considering the higher RH and LWC concentration at night, the increased concentrations of C_2 and related SOA during the nighttime may be closely linked to the accelerated aqueous production (Cheng et al., 2015; Meng et al., 2020).

The molecular pattern of TDOCs was predominated by C_2 followed by C_4 and C_3 as discussed above, consistent with the molecular distribution in biomass burning smoke (Kawamura et al., 2013; Kundu et al., 2010; Meng et al., 2020; Sorathia et al., 2018). To explore the contribution of biomass burning to TDOCs, levoglucosan, and K^+ were proposed as reliable markers for biomass burning (Hoffmann et al., 2010; Huang et al., 2006). K^+ is abundant in aerosols emitted from biomass burning (Andreae, 1983), thus K^+ exhibited a close correlation with levoglucosan (R^2=0.77, Table S1) before the LCD. There was no obvious diurnal difference of levoglucosan and K^+ between daytime (140 ± 54.9 ng m^{-3}, 2.0 ± 0.1 μg m^{-3}) and nighttime (141 ± 84.4 ng m^{-3}, 2.1 ± 0.4 μg m^{-3}), suggesting that the higher concentrations of C_2 and related SOA at night were irrelevant to the difference in the emission strength of organic precursors from biomass burning in the daytime and nighttime. C_2, diacids, and TDOCs exhibited strong correlations with levoglucosan and K^+ before the LCD ($R^2 > 0.5$), while such correlations were not observed during the LCD ($R^2 < 0.2$, Table S1), suggesting that biomass burning was an essential contributor to C_2 and related SOA before the LCD rather than during the LCD. The ratio of C_2/levoglucosan (1.7 ± 0.6) at night before the LCD exhibited a larger value than that (1.3 ± 0.5) in the day, which was mainly ascribed to the accelerated aqueous formation of C_2 at night. Moreover, the mean values of C_2/levoglucosan (1.5 ± 0.6), C_2/K^+ (0.2 ± 0.03), C_4/levoglucosan (0.4 ± 0.1), and C_4/K^+ (0.05 ± 0.02) ratios before the LCD were higher than those (0.05, 0.05, 0.03, and 0.03) in fresh particles emitted from savanna fires of southern African (Gao et al., 2003). It is interesting to note that the average ratios of C_2/C_4 (3.9 ± 1.5), C_3/C_4 (0.3 ± 0.1), and C_2/diacids (0.52 ± 0.55) before the LCD were almost equal to those (3.8, 0.3, and 0.55) measured in the aerosols for two days aging biomass samples via chamber experiments (Shen et al., 2022), suggesting that C_2 and related SOA before the LCD were linked tightly to the secondary oxidation of organic precursors emitted from biomass burning.

To explore the formation pathways and contributing factors of C_2 and related SOA before the LCD, the temporal variations of major diacids, LWC, pH_{is}, and meteorological parameters (e.g., solar radiation, temperature, and RH) were illustrated in Fig. 5. The SO_4^{2-} formation was largely from aqueous phase oxidation (see Text S5), thus the correlation analysis between SO_4^{2-} and C_2 can be used to evaluate the formation process of C_2 mainly via aqueous phase pathways (Sorathia et al., 2018). C_2 was correlated significantly with SO_4^{2-} in the daytime (R^2 = 0.53) and nighttime (R^2 = 0.66) (Fig. S2) before the LCD, confirming the dominant aqueous-phase formation pathway of C_2. It is worth noting that the slope of the regression line of C_2/SO_4^{2-} ratio (0.005) at night was 1.3 times higher than that (0.004) during the daytime (Fig. S2). Both the higher slope and C_2 concentrations indicate a more efficient formation of C_2 at night, largely because the C_2 production requires multiple steps of aqueous oxidation from VOCs while the formation of SO_4^{2-} requires fewer steps (Miyazaki et al., 2009). Noticeably, the concentrations of C_2 and diacids, as well as C_2/diacids ratio culminated on the nighttime of January 23, which was characterized by significantly higher LWC concentration (172 μg m^{-3}) and RH (86.9%) (Fig. 5). Gly and mGly are gaseous oxidation products of biogenic and anthropogenic VOCs with OH ·radicals, and both are highly water-soluble and thus can dissolve in the aqueous phase (Carlton et al., 2006; Myriokefalitakis et al., 2011). The correlations of the concentrations of Gly, mGly, and C_2 with OH ·radicals were not straightforward ($p > 0.05$, Fig. S4), primarily because of the multiple sources (e.g., biomass burning, fossil fuel combustion, and other sources except for the aqueous OH ·radical oxidation pathway) of C_2 (Cao et al., 2017; Narukawa et al., 1999; Xu et al., 2022) and the complexity of the local atmospheric environment. In addition, the equilibrium concentrations of each component varied continuously with their molar fractions in the aerosol phase during the reaction process, thus C_2 was not necessarily correlated directly with OH · radicals. The higher RH and

LWC concentration were favorable for the partitioning of Gly and mGly from gaseous phase to aqueous phase and forming C_2. As shown in Fig. 5, the enhanced concentrations of Gly and mGly in $PM_{2.5}$ before the LCD were observed when RH and LWC increased. Thus, C_2 and its precursors (including Gly and mGly) were positively correlated with RH and LWC, respectively ($R^2 > 0.45$, Fig. 4a). Moreover, the ratios of C_2/Gly and C_2/mGly also showed a significant correlation with RH and LWC ($R^2 > 0.4$, Fig. 4a). Indeed, the increase in C_2 (increased by 1.9 times) was significantly higher than that of Gly (increased by 1.1 times) and mGly (increased by 1.2 times) with the increase of LWC before the LCD. These discussions suggest that the higher LWC concentration and RH could promote the aqueous-phase formation of C_2 from Gly and mGly. Therefore, C_2 before the LCD was mainly derived from the aqueous production where LWC and RH appeared to be vitally important controlling factors as supported by positive matrix factorization (PMF) results that will be discussed in Section 3.6. The nighttime concentrations of LWC and RH were higher than those during the daytime, which led to the higher concentration and percentage contribution of C_2 in the nighttime.

Previous studies have reported that C_2 can also be derived from the chain-breaking of longer-chain diacids in the aqueous phase (Kawamura and Usukura, 1993; Miyazaki et al., 2009). However, there was moderate or no serious correlation between C_2 and longer-chain diacids (e.g., C_3 and C_4), respectively ($R^2 < 0.3$, Fig. 4a). Furthermore, longer-chain diacids and the ratios of C_2/C_3 and C_2/C_4 exhibited no significant correlation with LWC or RH ($R^2 < 0.24$, Fig. 4a). It can be concluded the effect of chain-breaking of longer homologous diacids on aqueous mechanism of C_2 was negligible in this study. Numerous studies have reported that the acidic condition of aerosol is beneficial to the BSOA formation such as 2-methylglyceric acid from BVOCs (e.g., isoprene), and ultimately be transformed into C_2 via Gly, mGly, and ωC_2 in the aqueous phase by acid-catalyzed oxidation reactions (Surratt et al., 2007). Laboratory experiment has pointed out that the acidic environment of aerosol can accelerate the uptake and production of Gly and mGly via acidic-catalyzed heterogeneous oxidation (Jang et al., 2002; Surratt et al., 2007). As shown in Fig. 4a, pH_{is} exhibited pronounced negative relationships with C_2 and its precursors such as Gly and mGly ($R^2 \geq 0.45$), which was also found in other field studies (Cheng et al., 2017; Meng et al., 2014; Wang et al., 2017; Yu et al., 2021). Such negative correlations were possibly because more SO_2 could lead to more SO_4^{2-} and lower pH_{is}, which in turn enhanced the solubility of Gly and mGly and ultimately promoted C_2 formation. Therefore, an acid-catalyzed C_2 formation may occur in the aqueous phase under the present atmospheric conditions before the LCD. However, Tan et al. (2009) reported that acidity had a minor effect on C_2 formation at cloud- and fog-relevant conditions via online experiments. Wang et al. (2015) suggested that the coarse particles during the dust period, which are alkaline, are favorable for the C_2 formation from ωC_2, largely because the reaction rate constant (3.6×10^8 M^{-1} s^{-1}) of ωC_2 with OH ·radical to form C_2 is smaller than that (2.9×10^9 M^{-1} s^{-1}) of its anion, glyoxylate. At very acidic pH, C_2 is not only formed more slowly but also oxidized more slowly (Eugene et al., 2016; Herrmann, 2003). Those findings conflicted with each other, probably because the concentration levels of organic precursors, acidity, LWC, and other influencing factors were different from the cases in our field observations, thus further studies are necessary to elucidate the influencing mechanism of acidity on C_2 formation.

3.4 Enhanced gaseous photochemical formation of diacids and related species during the LCD

Being different from the time period before the LCD, the strong correlations of C_2, Gly, mGly, and ratios of C_2/Gly and C_2/mGly were not obtained with RH or LWC ($R^2 < 0.2$) during the LCD (Fig. 4b), suggesting the insignificant effect of the aqueous-phase formation on C_2 during the LCD. As discussed in Section 3.2, the concentrations of C_2, diacids, and TDOCs as well as the ratio of C_2/diacids during the LCD were higher than those before the LCD, despite the anthropogenic source strength dropping dramatically during the LCD. Given the higher O_3 concentration and stronger solar radiation during the LCD (Table 1), it can be expected that the enhanced concentration and contribution of C_2 were driven by the promoted photochemical oxidation, which was supported by the significantly higher C_3/C_4 ratio (1.6 ± 0.4) during the LCD than that (0.3 ± 0.1) before the LCD. Since C_3 can be generated from photochemical oxidation of C_4 in the atmosphere (Kawamura

and Bikkina, 2016), the relatively high C_3/C_4 ratio during the LCD (Fig. 3b) indicates that aerosols during the LCD experienced more substantial photochemical aging. Field measurements and chamber experiments have reported that C_2 can be principally originated from photochemical oxidation of α-dicarbonyls from VOCs driven by O_3 and OH ·radicals (Meng et al., 2021; Mochizuki et al., 2017). Bikkina et al. (2021) reported a laboratory production of C_2 and other LMW diacids together with intermediate oxoacids and α-dicarbonyls by ozonolysis of isoprene. O_3 was used here as a marker for the oxidant concentration of gaseous photochemical oxidation. In addition, solar radiation could also be used as a reliable proxy for gaseous photochemical productions of C_2 and other diacids (Deshmukh et al., 2018). In view of the significant enhancement of oxidant concentration (e.g., O_3 and OH ·radicals) and solar radiation during the LCD, it could be concluded that the production of C_2 and related compounds may be driven by the higher oxidant concentrations.

To investigate the formation mechanism and potential sources of C_2 and related compounds during the LCD, the temporal variations in C_2 and its precursors, O_3, as well as meteorological factors are presented in Fig. 5. It is interesting to note that the highest O_3 concentration was observed on the daytime of January 31 when the concentrations of C_2 and diacids reached their peaks. Moreover, both C_2 and diacids concentrations as well as the C_2/diacids ratio exhibited robust correlations with O_3 ($R^2 > 0.5$, Fig. 4b), respectively, suggesting that O_3 or related oxidants may have played an important role in the formation of C_2 and other diacids. Additionally, C_2 and diacids concentrations exhibited similar patterns of variations (Fig. 5) and strong correlations ($R^2 > 0.5$, Fig. 4b) with solar radiation during the daytime. However, such similarities and strong correlations of those were not observed with temperature ($R^2 < 0.2$, Fig. 4b and Fig. 5), again suggesting that the effect of temperature on the loss of C_2 and diacids was negligible. These results confirmed that C_2 and other diacids were overwhelmingly derived from the gaseous photochemical processes driven by the stronger solar radiation, O_3, and other oxidants such as OH ·radicals.

A number of studies have demonstrated that the longer-chain diacids can be photochemically degraded into C_2 (Kawamura and Bikkina, 2016; Zhao et al., 2020). It is worth noting that C_2 was correlated strongly with longer-chain diacids such as C_3 and C_4, respectively ($R^2 > 0.5$, Fig. 4b). The ratio of C_2/diacids was correlated strongly with the ratios of C_3/C_4 ($R^2 = 0.68$) and C_2/C_4 ($R^2 = 0.58$, Fig. 4b), indicating that C_2 during the LCD may be largely derived from the photochemical degradation of higher molecular weight homologues of diacids. However, the correlation of the C_2/diacids ratio with (C_3–C_{11})-C/WSOC ($R^2 = 0.12$) was weak, primarily because the supply rates of longer-chain diacids are faster than their degradation rates in C_2 formation (Zhao et al., 2020). C_2/diacids ratio was correlated robustly with solar radiation during the daytime ($R^2 = 0.76$, Fig. 4b). Previous study suggested that the correlation analysis of C_2/diacids, C_2/C_4, and C_3/C_4 with O_3 could indicate the photochemical chain-breaking of longer-chain diacids producing C_2 (Liu et al., 2021). These ratios were observed to be correlated significantly with O_3 ($R^2 > 0.45$, Fig. 4b). These results confirm that C_2 during the LCD was primarily originated from the photochemical degradation of longer-chain homologous diacids driven by stronger solar radiation and higher O_3 concentration and other oxidants rather than higher temperature, which was further supported by the results of stable carbon isotopic composition of diacids (discussed in Section 3.5) and PMF analysis (discussed in Section 3.6).

3.5 Stable carbon isotopic compositions of diacids and related species before and during the LCD

The $\delta^{13}C$ values of specific organic acids can provide insights into the sources and photochemical aging (or processing) of organic aerosols due to the isotopic fractionation of carbon during the phase partitioning and/or photochemical oxidation (Wang et al., 2020a; Zhang et al., 2016). Thus, we investigated the stable carbon isotopic compositions of major diacid homologues to further discuss the atmospheric processes of diacid homologues and evaluate the aging degree of organic aerosols before and during the LCD.

On average, most of the detected diacid homologues exhibited higher $\delta^{13}C$ values during the LCD than those before the LCD (Table 3, Fig. 6). A previous study demonstrated that the enriched $\delta^{13}C$ values in diacid homologues were found with UV

irradiation time (Pavuluri and Kawamura, 2016). Additionally, Shen et al. (2022) reported that the $\delta^{13}C$ value of C_2 in the 7-d aged biomass samples was higher than in the 2-d aged biomass samples using the combustion chamber. Thus, the enrichment of $\delta^{13}C$ values in diacid homologues during the LCD was mainly due to the promoted photochemical oxidation during the LCD. Similar to the diurnal variations in major diacids' concentrations, the nighttime $\delta^{13}C$ values of these detected diacids were more positive (or more negative) than those in the daytime before (or during) the LCD, which was ascribed to their different sources and formation processes in these two observation periods. In brief, the $\delta^{13}C$ values exhibited a decreasing trend as the carbon numbers of diacids increased (Fig. 6), consistent with other observation campaigns elsewhere (Meng et al., 2020; Pavuluri and Kawamura, 2016; Wang and Kawamura, 2006). The mean $\delta^{13}C$ value (−20 ± 2.5‰) of C_2 was the highest in each period (Table 3), which was comparable to that (−20 ± 3.5‰) observed in its surrounding city such as Liaocheng (Meng et al., 2020), and higher than the values obtained in other China's megacities such as Beijing (−23 ± 3.4‰) (Zhao et al., 2018) and Xi'an ($PM_{2.1}$: from −21 to −24‰) (Wang et al., 2012), but smaller than the values measured in the Korea Climate Observatory at Gosan (−16 ± 4.3‰) of East Asia (Zhang et al., 2016) and western Pacific and Southern Ocean (−17 ± 0.8‰) (Wang and Kawamura, 2006) in the winter (Fig. 7). It is worth noting that the average $\delta^{13}C$ value of C_2 (−22 ± 1.9‰) before the LCD was equal to that (−22 ± 1.2‰) determined in the 2-d biomass samples (Shen et al., 2022) (Fig. 7), confirming that biomass burning and subsequent oxidation exerted an important effect on C_2 before the LCD.

As mentioned above, C_2 can be not only originated from the photochemical breakdown (or decomposition) of C_3 and C_4 via kC_3 and hydroxymalonic acids (hC_4), but also be derived from the photochemical oxidation of aromatic hydrocarbons via ωC_2. The positive correlations of the ^{13}C values of C_2 with mass ratios of $C_2/\omega C_2$ ($R^2 \geq 0.39$) and C_2/kC_3 ($R^2 \geq 0.37$) during the LCD were observed, whereas such robust relations only with $C_2/\omega C_2$ ($R^2 \geq 0.47$) rather than C_2/kC_3 ($R^2 \geq 0.01$) before the LCD were observed (Fig. 8). These results imply that the effect of photochemical decomposition of higher diacid homologues on C_2 before the LCD was minor, consistent with the discussions in Section 3.3. The isotopic values of diacids followed the order of $C_2 > C_3 > C_4$ in each time period (Fig. 6), primarily because diacids containing more carbon numbers may be more reactive to oxidants such as O_3 and OH radicals in the atmosphere (Aggarwal and Kawamura, 2008). On the other hand, the removal of CO_2/CO in the processes of C_3 and C_4 reacting with atmospheric oxidants can generate more ^{13}C-enriched C_2 due to the KIEs (Wang and Kawamura, 2006). The isotopic values of C_9 ranged from −25 to −30‰ before the LCD, whose difference was less distinguished than those of C_2−C_4 (Table 3). It is worth noting that the $\delta^{13}C$ values of organic species from marine plankton (−20‰) are higher than those from terrestrial higher plants (C_3 plants: −27‰). The $\delta^{13}C$ values of C_9 and the strong correlation of C_9 with levoglucosan before the LCD as discussed above indicate that biomass burning emitting unsaturated fatty acids and subsequent aqueous oxidation was an important contributor to C_9 in Jinan during the wintertime. The most negative $\delta^{13}C$ value among the identified organic species was tPh throughout the entire period, whose $\delta^{13}C$ value (−35 ± 3.1‰) was approximately equal to that (−35 ± 5.3‰) in Liaocheng (Meng et al., 2020) and lighter than that (−34 ± 3.4‰) in Beijing (Zhao et al., 2018) of China where the primary emissions from the combustion of plastic wastes is an essential source of tPh. Moreover, the $\delta^{13}C$ value of tPh was negatively (one outlier that possessed a relatively high relative abundance of tPh in diacids was removed) in the daytime or poorly correlated with the ratio of tPh/diacids at night before the LCD (Fig. 8f). The $\delta^{13}C$ value of tPh presented a negative correlation with the tPh/diacids during the LCD (Fig. 8l). These results suggest that the primary sources of plastic wastes burning exerted a significant impact on tPh in the atmosphere of Jinan.

Similarly, the $\delta^{13}C$ value of oxoacids increases as carbon number decreases (Table 3, Fig. 6). ωC_2 has the highest $\delta^{13}C$ value, followed by Pyr, and ωC_3 before and during the LCD. The lighter isotope (^{12}C) was more enriched in ωC_2 than both Gly and mGly (Table 3) in each time period. ωC_2 is largely derived from the photochemical oxidation of organic precursors such as α-dicarbonyls and acetic acid (Carlton et al., 2007). ^{12}C can be preferentially accumulated in the products in the non-reversible chemical processes (Wang et al., 2012), resulting in the lighter $\delta^{13}C$ values of ωC_2 than its precursors. mGly

was less enriched in ^{13}C than Gly (Table 3, Fig. 6) in each time period, attributed to the lower vapor pressure and higher carbon numbers of mGly that may lead to the weaker isotopic fractionation (Zhang et al., 2016).

It is well established that the ^{13}C values of diacids and related compounds become isotopically heavier in the aging process of organic aerosols (Pavuluri and Kawamura, 2016; Zhang et al., 2016). As mentioned above, the ratios of C_2/Gly, C_2/mGly, and C_2/diacids are usually considered significant proxies to evaluate the aging of organic aerosols. These ratios exhibited strong correlations with the ^{13}C values of C_2 in each period ($R^2 > 0.4$, Fig. 8), indicating the production of more ^{13}C-enriched C_2 during the aging processes. The less depletion of ^{13}C in C_2 of aged organic aerosols conformed to the actual secondary KIE on activated H-atom abstraction by OH radicals rather than to the mass dependence of collision frequencies in the gas phase (Enami et al., 2015). Organic species can react with OH radicals and other atmospheric oxidants in the atmospheric oxidation reactions, which result in the removal of CO_2/CO containing ^{12}C and cause the oxidation products more enriched with the heavier isotope ^{13}C (Narukawa et al., 1999). Therefore, the ^{13}C values of major diacids and the related compounds during the LCD were less negative than those before the LCD, again demonstrating that the gaseous photochemical oxidation was promoted during the LCD because of the higher temperature and O_3 concentration under the clearer sky conditions, which was in agreement with the results in Section 3.2.

3.6 Comparison of the source fingerprinting before and during the LCD

To further quantitatively analyze the crucial sources and their relative contributions of diacids and related compounds, PMF was adopted. Detailed information about PMF analysis was described in Text S3. The model stability of the five-factor solution and error estimation diagnostics were detailed in Table S5 and Table S6, respectively. The PMF-resolved source profiles for the five factors before and during the LCD were shown in Fig. 9. Before the LCD, C_2, C_3, ωC_2, Pyr, Gly, mGly, LWC, WSOC, NO_3^-, SO_4^{2-}, and NH_4^+ exhibited the relatively higher loadings in the first factor (Fig. 9a). SO_4^{2-} is a representative product of secondary oxidation in the aqueous phase, and LWC had been proved to be a significant influencing factor during the aqueous oxidation as discussed above. Therefore, the first factor was considered the sources from aqueous phase oxidation. The second factor was characterized by the stronger loadings of C_3, C_4, Ph, and EC. Ph is generated from the photochemical oxidation of polycyclic aromatic hydrocarbons (e.g., naphthalene) that are primarily emitted from the domestic coal combustion in China's megacities (Zhao et al., 2018), thus the second factor was categorized as a coal combustion source. O_3 had been confirmed to be a reliable proxy for gaseous photochemical oxidation, thus the robust relationships of O_3, α-dicarbonyls, and ωC_2 with the third factor indicated the contribution of gaseous photochemical oxidation. The fourth factor was significantly associated with Mg^{2+} and Ca^{2+}, which represented dust emission. As an important indicator of biomass burning, levoglucosan was strongly correlated with C_9 and EC in the fifth factor. Although diacids and related compounds can be produced from the secondary oxidation of organic precursors from biomass burning (Cao et al., 2017; Kawamura et al., 2013), biomass burning can directly emit those compounds (Fu et al., 2008; Gao et al., 2003; Kundu et al., 2010; Narukawa et al., 1999; Shen et al., 2022). Thus, the fifth factor could be regarded as a primary source of biomass burning.

During the LCD, the first factor was dominated by O_3, major diacids, and α-dicarbonyls (Fig. 9b), which represented gaseous photochemical oxidation. The second factor was strongly correlated with C_2, C_4, LWC, WSOC, NO_3^-, SO_4^{2-}, and NH_4^+, suggesting a significant contribution of aqueous oxidation. Levoglucosan, C_9, EC, and OC presented the stronger loadings in the third factor, indicating a primary source of biomass burning. Mg^{2+} and Ca^{2+} exhibited strong correlations with the fourth factor, suggesting the sources from dust emission. Ph and EC presented strong correlations with the fifth factor, representing a coal combustion source. The PMF-resolved relative contributions to the detected species before and during the LCD were presented in Fig. 9c and Fig. 9d, respectively. The aqueous oxidation made the greatest contribution (47.2%) to C_2 and related compounds, while the gaseous photochemical oxidation contributed only 12.3% to the total determined sources before the LCD, again suggesting that the aqueous oxidation was the dominant formation pathway for these organic

compounds before the LCD as discussed in Section 3.3. However, the gaseous photochemical oxidation contributed the largest percentage (50.5%) to the total identified sources, while the aqueous oxidation accounted for only 16.1% of the total identified sources during the LCD, confirming that the gaseous photochemical oxidation exerted a leading role in the formation of homologous diacids during the LCD, which was in agreement with the results as discussed in Section 3.4. The lower contribution of C_2 and related compounds from aqueous oxidation during the LCD was likely because of the decrease of RH and LWC. The contribution of biomass burning increased from 11.4% before the LCD to 13.6% during the LCD. However, the contribution of coal combustion decreased from 16.2% before the LCD to 7.2% during the LCD, largely because of the decreased usage of coal for the industry.

4 Summary and conclusions

This work has investigated the effects of variations in anthropogenic emissions and meteorological conditions on the formation pathways and influencing factors of diacidis and related compounds by taking advantage of COVID-19 LCD as a "controlled experiment". While previous studies focused on the importance of higher emission level and promoted secondary oxidation for producing more diacids and related compounds, this study strongly suggested that the enhanced secondary formation of diacids and related species could offset the significant decline of organic precursors from anthropogenic pollutant emissions during the LCD. The sources and formation mechanisms of C_2 and diacids before and during the LCD were illustrated in Fig. 10. Before the LCD, higher RH and hygroscopic particles (e.g., SIA) led to an increase in LWC, which promoted the partitioning of water-soluble organic precursors (e.g., Gly and mGly) from the gaseous phase into the aqueous phase, thereby enhancing the aqueous formation of C_2 (Fig. 10). During the LCD, C_2 was derived from the photochemical degradation of longer-chain diacids (e.g., C_3 and C_4) that was driven by the stronger solar radiation and higher O_3 concentration and other oxidants (Fig. 10). In this study, we for the first time successfully quantified the relative contributions of aqueous-phase oxidation and gaseous-phase photochemical oxidation to the ambient C_2 and related species, which were 47.2% and 12.3% before the LCD and 16.1% and 50.5% during the LCD, respectively. The reactivity of ^{13}C was higher than that of ^{12}C in the gaseous photochemical oxidation, leading to higher $\delta^{13}C$ values of C_2 during the LCD than before the LCD (Fig. 10). Furthermore, more enriched ^{13}C in C_2 was observed during the aging processes of organic aerosols. To the best of our knowledge, this study was first conducted on the effect of OH · radicals on C_2 formation in the field campaign, though many studies have been performed in chamber experiments. We observed that C_2 was not necessarily correlated directly with OH · radicals in the aqueous oxidation, possibly due to the fact that C_2 has multiple sources (e.g., biomass burning and fossil fuel combustion) and the complexity of local atmospheric environment, which still needs to be elucidated by more field observations. These results are helpful for better understanding the sources, formation processes, and driving factors of SOA in the urban regions of East China. Nevertheless, our study suggested that, even if the primary emissions are practically reduced, we cannot completely solve the current air pollution problem in the North China Plain where the sources and precursors of secondary aerosols are extremely complicated. The balanced strategy and trans-regional joint control of major air pollutants are necessary to be considered together with meteorological conditions.

Overall, we obtained that the sources, formation mechanisms, and aging processes of SOA differed significantly during different time periods even at the same observation site. It is needed to conduct more field observations of SOA regarding the types of precursors, formation pathway via aqueous oxidation and gaseous photochemical oxidation, and aging level at different sites and in different time periods to improve the accuracy of aerosol models and informing policy about effective air quality measures.

Data availability. The data in this study are available at: https://doi.org/10.5281/zenodo.7533247 (Meng et al., 2023).

Author contribution. PF designed the study. YW, YL, TH, and MC carried out the experiments and performed the data analysis. HZ and KL estimated the OH ·radical concentration. JM prepared the manuscript with contributions from all co-authors.

Competing interests. The authors have the following competing interests: One of the coauthors, Prof. Kimitaka Kawamura is one of the editorial members of this journal.

Acknowledgments. This work was supported by the National Natural Science Foundation of China (Grant No. 42177083), the Natural Science Foundation of Shandong Province (Grant No. ZR2020MD113), the Junior Faculty Support Program for Scientific and Technological Innovations in Shandong Provincial Higher Education Institutions (2021KJ085), and the Open Funds of State Key Laboratory of Loess and Quaternary Geology, Institute of Earth Environment, Chinese Academy of Sciences (Grant No. SKLLOG2020).

References

Aggarwal, S. G. and Kawamura, K.: Molecular distributions and stable carbon isotopic compositions of dicarboxylic acids and related compounds in aerosols from Sapporo, Japan: Implications for photochemical aging during long-range atmospheric transport, J. Geophys. Res. Atmos., 113, D14301, 10.1029/2007jd009365, 2008.

Andreae, M. O.: Soot Carbon and Excess Fine Potassium: Long-Range Transport of Combustion-Derived Aerosols, Science, 220, 1148, 1983.

Bao, R. and Zhang, A.: Does lockdown reduce air pollution? Evidence from 44 cities in northern China, Sci. Total Environ.,731, 139052, https://doi.org/10.1016/j.scitotenv.2020.139052, 2020.

Bikkina, S., Kawamura, K., and Miyazaki, Y.: Latitudinal distributions of atmospheric dicarboxylic acids, oxocarboxylic acids, and α-dicarbonyls over the western North Pacific: Sources and formation pathways, J. Geophys. Res. Atmos., 120, 5010-5035, 10.1002/2014jd022235, 2015.

Bikkina, S., Kawamura, K., Sakamoto, Y., and Hirokawa, J.: Low molecular weight dicarboxylic acids, oxocarboxylic acids and α-dicarbonyls as ozonolysis products of isoprene: Implication for the gaseous-phase formation of secondary organic aerosols, Sci. Total Environ., 769, 144472, https://doi.org/10.1016/j.scitotenv.2020.144472, 2021.

Buxton, G., N. Malone, T., and Arthur Salmon, G.: Oxidation of glyoxal initiated by OH in oxygenated aqueous solution, Journal of the Chemical Society, Faraday Transactions, 93, 2889-2891, 10.1039/A701468F, 1997.

Cao, F., Zhang, S.-C., Kawamura, K., Liu, X., Yang, C., Xu, Z., Fan, M., Zhang, W., Bao, M., Chang, Y., Song, W., Liu, S., Lee, X., Li, J., Zhang, G., and Zhang, Y.-L.: Chemical characteristics of dicarboxylic acids and related organic compounds in PM2.5 during biomass-burning and non-biomass-burning seasons at a rural site of Northeast China, Environ. Pollut., 231, 654-662, https://doi.org/10.1016/j.envpol.2017.08.045, 2017.

Carlton, A. G., Turpin, B. J., Lim, H.-J., Altieri, K. E., and Seitzinger, S.: Link between isoprene and secondary organic aerosol (SOA): Pyruvic acid oxidation yields low volatility organic acids in clouds, Geophys. Res. Lett., 33, L06822, 10.1029/2005gl025374, 2006.

Carlton, A. G., Turpin, B. J., Altieri, K. E., Seitzinger, S., Reff, A., Lim, H.-J., and Ervens, B.: Atmospheric oxalic acid and SOA production from glyoxal: Results of aqueous photooxidation experiments, Atmos. Environ., 41, 7588-7602, http://dx.doi.org/10.1016/j.atmosenv.2007.05.035, 2007.

Cheng, C., Li, M., Chan, C. K., Tong, H., Chen, C., Chen, D., Wu, D., Li, L., Wu, C., Cheng, P., Gao, W., Huang, Z., Li, X., Zhang, Z., Fu, Z., Bi, Y., and Zhou, Z.: Mixing state of oxalic acid containing particles in the rural area of Pearl River Delta, China: implications for the formation mechanism of oxalic acid, Atmos. Chem. Phys., 17, 9519-9533, 10.5194/acp-17-9519-2017, 2017.

Cheng, C., Wang, G., Meng, J., Wang, Q., Cao, J., Li, J., and Wang, J.: Size-resolved airborne particulate oxalic and related

secondary organic aerosol species in the urban atmosphere of Chengdu, China, Atmos. Res., 161–162, 134-142, http://dx.doi.org/10.1016/j.atmosres.2015.04.010, 2015.

Cheng, C., Wang, G., Zhou, B., Meng, J., Li, J., Cao, J., and Xiao, S.: Comparison of dicarboxylic acids and related compounds in aerosol samples collected in Xi'an, China during haze and clean periods, Atmospheric Environment, 81, 443-449, http://dx.doi.org/10.1016/j.atmosenv.2013.09.013, 2013.

Chow, J. C., Watson, J. G., Chen, L. W. A., Arnott, W. P., Moosmüller, H., and Fung, K.: Equivalence of Elemental Carbon by Thermal/Optical Reflectance and Transmittance with Different Temperature Protocols, Environ. Sci. Technol., 38, 4414-4422, 10.1021/es034936u, 2004.

Crahan, K. K., Hegg, D., Covert, D. S., and Jonsson, H.: An exploration of aqueous oxalic acid production in the coastal marine atmosphere, Atmospheric Environment, 38, 3757-3764, http://dx.doi.org/10.1016/j.atmosenv.2004.04.009, 2004.

Deshmukh, D. K., Mozammel Haque, M., Kawamura, K., and Kim, Y.: Dicarboxylic acids, oxocarboxylic acids and α-dicarbonyls in fine aerosols over central Alaska: Implications for sources and atmospheric processes, Atmos. Res., 202, 128-139, https://doi.org/10.1016/j.atmosres.2017.11.003, 2018.

Devineni, S. R., Pavuluri, C. M., Wang, S., Ren, L., Xu, Z., Li, P., Fu, P., and Liu, C.-Q.: Size-Resolved Characteristics and Sources of Inorganic Ions, Carbonaceous Components and Dicarboxylic Acids, Benzoic Acid, Oxocarboxylic Acids and α-Dicarbonyls in Wintertime Aerosols from Tianjin, North China, Aerosol Science and Engineering, 7, 1-22, 10.1007/s41810-022-00159-0, 2023.

Ding, Z., Du, W., Wu, C., Cheng, C., Meng, J., Li, D., Ho, K., Zhang, L., and Wang, G.: Summertime atmospheric dicarboxylic acids and related SOA in the background region of Yangtze River Delta, China: Implications for heterogeneous reaction of oxalic acid with sea salts, Sci. Total Environ., 757, 143741, https://doi.org/10.1016/j.scitotenv.2020.143741, 2021.

Enami, S., Hoffmann, M. R., and Colussi, A. J.: Stepwise Oxidation of Aqueous Dicarboxylic Acids by Gas-Phase OH Radicals, J. Phys., Chem. Lett., 6, 527-534, 10.1021/jz502432j, 2015.

Ervens, B., Feingold, G., Frost, G. J., and Kreidenweis, S. M.: A modeling study of aqueous production of dicarboxylic acids: 1. Chemical pathways and speciated organic mass production, J. Geophys. Res., 109, D15205, 10.1029/2003jd004387, 2004.

Ervens, B., Turpin, B. J., and Weber, R. J.: Secondary organic aerosol formation in cloud droplets and aqueous particles (aqSOA): a review of laboratory, field and model studies, Atmos. Chem. Phys., 11, 11069-11102, 10.5194/acp-11-11069-2011, 2011.

Eugene, A. J., Xia, S.-S., and Guzman, M. I.: Aqueous Photochemistry of Glyoxylic Acid, The Journal of Physical Chemistry A, 120, 3817-3826, 10.1021/acs.jpca.6b00225, 2016.

Fountoukis, C., and Nenes, A.: ISORROPIA II: a computationally efficient thermodynamic equilibrium model for K^+–Ca^{2+}–Mg^{2+}–NH_4^+–Na^+–SO_4^{2-}–NO_3^-–Cl^-–H_2O aerosols, Atmos. Chem. Phys., 7, 4639-4659, 10.5194/acp-7-4639-2007, 2007.

Fu, P., Kawamura, K., Usukura, K., and Miura, K.: Dicarboxylic acids, ketocarboxylic acids and glyoxal in the marine aerosols collected during a round-the-world cruise, Marine Chemistry, 148, 22-32, http://dx.doi.org/10.1016/j.marchem.2012.11.002, 2013.

Fu, T.-M., Jacob, D. J., Wittrock, F., Burrows, J. P., Vrekoussis, M., and Henze, D. K.: Global budgets of atmospheric glyoxal and methylglyoxal, and implications for formation of secondary organic aerosols, J. Geophys. Res., 113, D15303, 10.1029/2007jd009505, 2008.

Gao, S., Hegg, D. A., Hobbs, P. V., Kirchstetter, T. W., Magi, B. I., and Sadilek, M.: Water-soluble organic components in aerosols associated with savanna fires in southern Africa: Identification, evolution, and distribution, J. Geophys.

Res. Atmos., 108, 8491, 10.1029/2002jd002324, 2003.

Gaubert, B., Bouarar, I., Doumbia, T., Liu, Y., Stavrakou, T., Deroubaix, A., Darras, S., Elguindi, N., Granier, C., Lacey, F., Müller, J.-F., Shi, X., Tilmes, S., Wang, T., and Brasseur, G. P.: Global Changes in Secondary Atmospheric Pollutants During the 2020 COVID-19 Pandemic, Journal of Geophysical Research: Atmospheres, 126, e2020JD034213, https://doi.org/10.1029/2020JD034213, 2021.

Gligorovski, S., Grgić, I., Net, S., Böge, O., Iinuma, Y., Kahnt, A., Scheinhardt, S., Herrmann, H., and Wortham, H.: Light-induced multiphase chemistry of gas phase ozone on aqueous pyruvic and oxalic acids: Aerosol chamber study, AGU Fall Meeting Abstracts, 2010.

Herrmann, H.: Kinetics of Aqueous Phase Reactions Relevant for Atmospheric Chemistry, Chemical Reviews, 103, 4691-4716, 10.1021/cr020658q, 2003.

Ho, K. F., Cao, J. J., Lee, S. C., Kawamura, K., Zhang, R. J., Chow, J. C., and Watson, J. G.: Dicarboxylic acids, ketocarboxylic acids, and dicarbonyls in the urban atmosphere of China, J. Geophys. Res. Atmos., 112, D22S27, 10.1029/2006jd008011, 2007.

Ho, K. F., Ho, S. S. H., Lee, S. C., Kawamura, K., Zou, S. C., Cao, J. J., and Xu, H. M.: Summer and winter variations of dicarboxylic acids, fatty acids and benzoic acid in $PM_{2.5}$ in Pearl Delta River Region, China, Atmos. Chem. Phys., 11, 2197-2208, 10.5194/acp-11-2197-2011, 2011.

Huang, R.-J., Zhang, Y., Bozzetti, C., Ho, K.-F., Cao, J.-J., Han, Y., Daellenbach, K. R., Slowik, J. G., Platt, S. M., Canonaco, F., Zotter, P., Wolf, R., Pieber, S. M., Bruns, E. A., Crippa, M., Ciarelli, G., Piazzalunga, A., Schwikowski, M., Abbaszade, G., Schnelle-Kreis, J., Zimmermann, R., An, Z., Szidat, S., Baltensperger, U., Haddad, I. E., and Prévôt, A. S. H.: High secondary aerosol contribution to particulate pollution during haze events in China, Nature, 514, 218, 10.1038/nature13774, https://www.nature.com/articles/nature13774#supplementary-information, 2014.

Huang, X., Ding, A., Gao, J., Zheng, B., Zhou, D., Qi, X., Tang, R., Wang, J., Ren, C., Nie, W., Chi, X., Xu, Z., Chen, L., Li, Y., Che, F., Pang, N., Wang, H., Tong, D., Qin, W., Cheng, W., Liu, W., Fu, Q., Liu, B., Chai, F., Davis, S. J., Zhang, Q., and He, K.: Enhanced secondary pollution offset reduction of primary emissions during COVID-19 lockdown in China, Natl. Sci. Rev., 10.1093/nsr/nwaa137, 2020.

Jang, M., Czoschke, N. M., Lee, S., and Kamens, R. M.: Heterogeneous Atmospheric Aerosol Production by Acid-Catalyzed Particle-Phase Reactions, Science, 298, 814, 2002.

Jung, J., Tsatsral, B., Kim, Y. J., and Kawamura, K.: Organic and inorganic aerosol compositions in Ulaanbaatar, Mongolia, during the cold winter of 2007 to 2008: Dicarboxylic acids, ketocarboxylic acids, and α-dicarbonyls, Journal of Geophysical Research: Atmospheres, 115, D22203, 10.1029/2010jd014339, 2010.

Kang, M., Zhang, J., Zhang, H., and Ying, Q.: On the Relevancy of Observed Ozone Increase during COVID-19 Lockdown to Summertime Ozone and PM2.5 Control Policies in China, Environmental Science & Technology Letters, 8, 289-294, 10.1021/acs.estlett.1c00036, 2021.

Kawamura, K. and Bikkina, S.: A review of dicarboxylic acids and related compounds in atmospheric aerosols: Molecular distributions, sources and transformation, Atmos. Res., 170, 140-160, http://dx.doi.org/10.1016/j.atmosres.2015.11.018, 2016.

Kawamura, K. and Kaplan, I. R.: Motor exhaust emissions as a primary source for dicarboxylic acids in Los Angeles ambient air, Environ. Sci. Technol., 21, 105-110, 10.1021/es00155a014, 1987.

Kawamura, K. and Usukura, K.: Distributions of low molecular weight dicarboxylic acids in the North Pacific aerosol samples, J. Oceano., 49, 271-283, 10.1007/bf02269565, 1993.

Kawamura, K. and Watanabe, T.: Determination of Stable Carbon Isotopic Compositions of Low Molecular Weight Dicarboxylic Acids and Ketocarboxylic Acids in Atmospheric Aerosol and Snow Samples, Anal. Chem., 76, 5762-5768, 10.1021/ac049491m, 2004.

Kawamura, K. and Yasui, O.: Diurnal changes in the distribution of dicarboxylic acids, ketocarboxylic acids and dicarbonyls in the urban Tokyo atmosphere, Atmospheric Environment, 39, 1945-1960, http://dx.doi.org/10.1016/j.atmosenv.2004.12.014, 2005.

Kawamura, K., Tachibana, E., Okuzawa, K., Aggarwal, S. G., Kanaya, Y., and Wang, Z. F.: High abundances of water-soluble dicarboxylic acids, ketocarboxylic acids and α-dicarbonyls in the mountain aerosols over the North China Plain during wheat burning season, Atmos. Chem. Phys. , 13, 3695-3734, 10.5194/acpd-13-3695-2013, 2013.

Kundu, S., Kawamura, K., Andreae, T. W., Hoffer, A., and Andreae, M. O.: Molecular distributions of dicarboxylic acids, ketocarboxylic acids and α-dicarbonyls in biomass burning aerosols: implications for photochemical production and degradation in smoke layers, Atmos. Chem. Phys., 10, 2209-2225, 10.5194/acp-10-2209-2010, 2010.

Kunwar, B., Kawamura, K., Fujiwara, S., Fu, P., Miyazaki, Y., and Pokhrel, A.: Dicarboxylic acids, oxocarboxylic acids and α-dicarbonyls in atmospheric aerosols from Mt. Fuji, Japan: Implication for primary emission versus secondary formation, Atmospheric Research, 221, 58-71, https://doi.org/10.1016/j.atmosres.2019.01.021, 2019.

Le, T., Wang, Y., Liu, L., Yang, J., Yung, Y. L., Li, G., and Seinfeld, J. H.: Unexpected air pollution with marked emission reductions during the COVID-19 outbreak in China, Science, eabb7431, 10.1126/science.abb7431, 2020.

Li, L., Li, Q., Huang, L., Wang, Q., Zhu, A., Xu, J., Liu, Z., Li, H., Shi, L., Li, R., Azari, M., Wang, Y., Zhang, X., Liu, Z., Zhu, Y., Zhang, K., Xue, S., Ooi, M. C. G., Zhang, D., and Chan, A.: Air quality changes during the COVID-19 lockdown over the Yangtze River Delta Region: An insight into the impact of human activity pattern changes on air pollution variation, Sci. Total Environ., 732, 139282, https://doi.org/10.1016/j.scitotenv.2020.139282, 2020.

Li, K., Jacob, D. J., Liao, H., Shen, L., Zhang, Q., and Bates, K. H.: Anthropogenic drivers of 2013–2017 trends in summer surface ozone in China, Proceedings of the National Academy of Sciences, 116, 422, 10.1073/pnas.1812168116, 2019.

Li, X.-d., Yang, Z., Fu, P., Yu, J., Lang, Y.-c., Liu, D., Ono, K., and Kawamura, K.: High abundances of dicarboxylic acids, oxocarboxylic acids, and α-dicarbonyls in fine aerosols ($PM_{2.5}$) in Chengdu, China during wintertime haze pollution, Environmental Science and Pollution Research, 22, 12902-12918, 10.1007/s11356-015-4548-x, 2015.

Li, Z., Zhou, R., Wang, Y., Wang, G., Chen, M., Li, Y., Wang, Y., Yi, Y., Hou, Z., Guo, Q., and Meng, J.: Characteristics and sources of amine-containing particles in the urban atmosphere of Liaocheng, a seriously polluted city in North China during the COVID-19 outbreak, Environ. Pollut., 289, 117887, https://doi.org/10.1016/j.envpol.2021.117887, 2021a.

Li, Z., Zhou, R., Li, Y., Chen, M., Wang, Y., Huang, T., Yi, Y., Hou, Z., Meng, J., and Yan, L.: Characteristics and Sources of Organic Aerosol Markers in PM2.5, Aerosol and Air Quality Research, 21, 210180, 10.4209/aaqr.210180, 2021b.

Lim, Y. B., Tan, Y., and Turpin, B. J.: Chemical insights, explicit chemistry, and yields of secondary organic aerosol from OH radical oxidation of methylglyoxal and glyoxal in the aqueous phase, Atmos. Chem. Phys., 13, 8651-8667, 10.5194/acp-13-8651-2013, 2013.

Liu, Y. and Wang, T.: Worsening urban ozone pollution in China from 2013 to 2017 – Part 2: The effects of emission changes and implications for multi-pollutant control, Atmos. Chem. Phys., 20, 6323-6337, 10.5194/acp-20-6323-2020, 2020.

Liu, J., Zhou, S., Zhang, Z., Kawamura, K., Zhao, W., Wang, X., Shao, M., Jiang, F., Liu, J., Sun, X., Hang, J., Zhao, J., Pei, C., Zhang, J., and Fu, P.: Characterization of dicarboxylic acids, oxoacids, and α-dicarbonyls in PM2.5 within the urban boundary layer in southern China: Sources and formation pathways, Environ. Pollut., 285, 117185, https://doi.org/10.1016/j.envpol.2021.117185, 2021.

Lu, K., Guo, S., Tan, Z., Wang, H., Shang, D., Liu, Y., Li, X., Wu, Z., Hu, M., and Zhang, Y.: Exploring atmospheric free-radical chemistry in China: the self-cleansing capacity and the formation of secondary air pollution, National

Science Review, 6, 579-594, 10.1093/nsr/nwy073, 2019.

Lv, S., Wang, F., Wu, C., Chen, Y., Liu, S., Zhang, S., Li, D., Du, W., Zhang, F., Wang, H., Huang, C., Fu, Q., Duan, Y., and Wang, G.: Gas-to-Aerosol Phase Partitioning of Atmospheric Water-Soluble Organic Compounds at a Rural Site in China: An Enhancing Effect of NH3 on SOA Formation, Environ. Sci. Technol., 56, 3915-3924, 10.1021/acs.est.1c06855, 2022.

Meng, J., Liu, X., Hou, Z., Yi, Y., Yan, L., Li, Z., Cao, J., Li, J., and Wang, G.: Molecular characteristics and stable carbon isotope compositions of dicarboxylic acids and related compounds in the urban atmosphere of the North China Plain: Implications for aqueous phase formation of SOA during the haze periods, Sci. Total Environ., 705, 135256, https://doi.org/10.1016/j.scitotenv.2019.135256, 2020.

Meng, J., Li, Z., Zhou, R., Chen, M., Li, Y., Yi, Y., Ding, Z., Li, H., Yan, L., Hou, Z., and Wang, G.: Enhanced photochemical formation of secondary organic aerosols during the COVID-19 lockdown in Northern China, Sci. Total Environ., 758, 143709, https://doi.org/10.1016/j.scitotenv.2020.143709, 2021.

Meng, J., Wang, G., Hou, Z., Liu, X., Wei, B., Wu, C., Cao, C., Wang, J., Li, J., Cao, J., Zhang, E., Dong, J., Liu, J., Ge, S., and Xie, Y.: Molecular distribution and stable carbon isotopic compositions of dicarboxylic acids and related SOA from biogenic sources in the summertime atmosphere of Mt. Tai in the North China Plain, Atmos. Chem. Phys., 18, 15069-15086, 10.5194/acp-18-15069-2018, 2018.

Meng, J., Wang, G., Li, J., Cheng, C., Ren, Y., Huang, Y., Cheng, Y., Cao, J., and Zhang, T.: Seasonal characteristics of oxalic acid and related SOA in the free troposphere of Mt. Hua, central China: Implications for sources and formation mechanisms, Science of The Total Environment, 493, 1088-1097, http://dx.doi.org/10.1016/j.scitotenv.2014.04.086, 2014.

Miyazaki, Y., Aggarwal, S. G., Singh, K., Gupta, P. K., and Kawamura, K.: Dicarboxylic acids and water-soluble organic carbon in aerosols in New Delhi, India, in winter: Characteristics and formation processes, J. Geophys. Res. Atmos., 114, D19206, 10.1029/2009jd011790, 2009.

Mochizuki, T., Kawamura, K., Miyazaki, Y., Wada, R., Takahashi, Y., Saigusa, N., and Tani, A.: Secondary formation of oxalic acid and related organic species from biogenic sources in a larch forest at the northern slope of Mt. Fuji, Atmos. Environ., 166, 255-262, https://doi.org/10.1016/j.atmosenv.2017.07.028, 2017.

Myriokefalitakis, S., Tsigaridis, K., Mihalopoulos, N., Sciare, J., Nenes, A., Kawamura, K., Segers, A., and Kanakidou, M.: In-cloud oxalate formation in the global troposphere: a 3-D modeling study, Atmos. Chem. Phys., 11, 5761-5782, 10.5194/acp-11-5761-2011, 2011.

Narukawa, M., Kawamura, K., Takeuchi, N., and Nakajima, T.: Distribution of dicarboxylic acids and carbon isotopic compositions in aerosols from 1997 Indonesian forest fires, Geophys. Res. Lett., 26, 3101-3104, https://doi.org/10.1029/1999GL010810, 1999.

Pavuluri, C. M. and Kawamura, K.: Evidence for 13-carbon enrichment in oxalic acid via iron catalyzed photolysis in aqueous phase, Geophysical Research Letters, 39, L03802, 10.1029/2011gl050398, 2012.

Pavuluri, C. M. and Kawamura, K.: Enrichment of ^{13}C in diacids and related compounds during photochemical processing of aqueous aerosols: New proxy for organic aerosols aging, Sci. Rep., 6, 36467, 10.1038/srep36467, 2016.

Pavuluri, C. M., Kawamura, K., Tachibana, E., and Swaminathan, T.: Elevated nitrogen isotope ratios of tropical Indian aerosols from Chennai: Implication for the origins of aerosol nitrogen in South and Southeast Asia, Atmospheric Environment, 44, 3597-3604, https://doi.org/10.1016/j.atmosenv.2010.05.039, 2010.

Perri, M. J., Seitzinger, S., and Turpin, B. J.: Secondary organic aerosol production from aqueous photooxidation of glycolaldehyde: Laboratory experiments, Atmospheric Environment, 43, 1487-1497, https://doi.org/10.1016/j.atmosenv.2008.11.037, 2009.

Rinaldi, M., Decesari, S., Carbone, C., Finessi, E., Fuzzi, S., Ceburnis, D., O'Dowd, C. D., Sciare, J., Burrows, J. P.,

Vrekoussis, M., Ervens, B., Tsigaridis, K., and Facchini, M. C.: Evidence of a natural marine source of oxalic acid and a possible link to glyoxal, J. Geophys. Res. Atmos., 116, n/a-n/a, 10.1029/2011jd015659, 2011.

Shen, M., Ho, K. F., Dai, W., Liu, S., Zhang, T., Wang, Q., Meng, J., Chow, J. C., Watson, J. G., Cao, J., and Li, J.: Distribution and stable carbon isotopic composition of dicarboxylic acids, ketocarboxylic acids and α-dicarbonyls in fresh and aged biomass burning aerosols, Atmos. Chem. Phys., 22, 7489-7504, 10.5194/acp-22-7489-2022, 2022.

Shen, M., Qi, W., Guo, X., Dai, W., Wang, Q., Liu, Y., Zhang, Y., Cao, Y., Chen, Y., Li, L., Liu, H., Cao, J., and Li, J.: Influence of vertical transport on chemical evolution of dicarboxylic acids and related secondary organic aerosol from surface emission to the top of Mount Hua, Northwest China, Science of The Total Environment, 858, 159892, https://doi.org/10.1016/j.scitotenv.2022.159892, 2023.

Shi, Z., Song, C., Liu, B., Lu, G., Xu, J., Van Vu, T., Elliott Robert, J. R., Li, W., Bloss William, J., and Harrison Roy, M.: Abrupt but smaller than expected changes in surface air quality attributable to COVID-19 lockdowns, Sci. Adv.,7, eabd6696, 10.1126/sciadv.abd6696, 2021.

Sorathia, F., Rajput, P., and Gupta, T.: Dicarboxylic acids and levoglucosan in aerosols from Indo-Gangetic Plain: Inferences from day night variability during wintertime, Sci. Total Environ., 624, 451-460, https://doi.org/10.1016/j.scitotenv.2017.12.124, 2018.

Surratt, J. D., Lewandowski, M., Offenberg, J. H., Jaoui, M., Kleindienst, T. E., Edney, E. O., and Seinfeld, J. H.: Effect of Acidity on Secondary Organic Aerosol Formation from Isoprene, Environ. Sci. Technol., 41, 5363-5369, 10.1021/es0704176, 2007.

Tan, Y., Perri, M. J., Seitzinger, S. P., and Turpin, B. J.: Effects of Precursor Concentration and Acidic Sulfate in Aqueous Glyoxal−OH Radical Oxidation and Implications for Secondary Organic Aerosol, Environmental Science & Technology, 43, 8105-8112, 10.1021/es901742f, 2009.

Wang, G., Cheng, C., Meng, J., Huang, Y., Li, J., and Ren, Y.: Field observation on secondary organic aerosols during Asian dust storm periods: Formation mechanism of oxalic acid and related compounds on dust surface, Atmos. Environ., 113, 169-176, http://dx.doi.org/10.1016/j.atmosenv.2015.05.013, 2015.

Wang, G., Xie, M., Hu, S., Gao, S., Tachibana, E., and Kawamura, K.: Dicarboxylic acids, metals and isotopic compositions of C and N in atmospheric aerosols from inland China: implications for dust and coal burning emission and secondary aerosol formation, Atmos. Chem. Phys., 10, 6087-6096, 10.5194/acp-10-6087-2010, 2010.

Wang, G., Kawamura, K., Cheng, C., Li, J., Cao, J., Zhang, R., Zhang, T., Liu, S., and Zhao, Z.: Molecular Distribution and Stable Carbon Isotopic Composition of Dicarboxylic Acids, Ketocarboxylic Acids, and α-Dicarbonyls in Size-Resolved Atmospheric Particles From Xi'an City, China, Environ. Sci. Technol., 46, 4783-4791, 10.1021/es204322c, 2012.

Wang, G., Zhang, R., Gomez, M. E., Yang, L., Levy Zamora, M., Hu, M., Lin, Y., Peng, J., Guo, S., Meng, J., Li, J., Cheng, C., Hu, T., Ren, Y., Wang, Y., Gao, J., Cao, J., An, Z., Zhou, W., Li, G., Wang, J., Tian, P., Marrero-Ortiz, W., Secrest, J., Du, Z., Zheng, J., Shang, D., Zeng, L., Shao, M., Wang, W., Huang, Y., Wang, Y., Zhu, Y., Li, Y., Hu, J., Pan, B., Cai, L., Cheng, Y., Ji, Y., Zhang, F., Rosenfeld, D., Liss, P. S., Duce, R. A., Kolb, C. E., and Molina, M. J.: Persistent sulfate formation from London Fog to Chinese haze, P. Natl. Acad. Sci. USA, 113, 13630-13635, 10.1073/pnas.1616540113, 2016.

Wang, H. and Kawamura, K.: Stable carbon isotopic composition of low-molecular-weight dicarboxylic acids and ketoacids in remote marine aerosols, J. Geophys. Res. Atmos., 111, https://doi.org/10.1029/2005JD006466, 2006.

Wang, J., Wang, G., Wu, C., Li, J., Cao, C., Li, J., Xie, Y., Ge, S., Chen, J., Zeng, L., Zhu, T., Zhang, R., and Kawamura, K.: Enhanced aqueous-phase formation of secondary organic aerosols due to the regional biomass burning over North China Plain, Environ. Pollut., 256, 113401, https://doi.org/10.1016/j.envpol.2019.113401, 2020a.

Wang, N., Xu, J., Pei, C., Tang, R., Zhou, D., Chen, Y., Li, M., Deng, X., Deng, T., Huang, X., and Ding, A.: Air Quality During COVID-19 Lockdown in the Yangtze River Delta and the Pearl River Delta: Two Different Responsive Mechanisms to Emission Reductions in China, Environmental Science & Technology, 55, 5721-5730, 10.1021/acs.est.0c08383, 2021.

Wang, P., Chen, K., Zhu, S., Wang, P., and Zhang, H.: Severe air pollution events not avoided by reduced anthropogenic activities during COVID-19 outbreak, Resour. Conserv. Recy., 158, 104814, https://doi.org/10.1016/j.resconrec.2020.104814, 2020b.

Warneck, P.: In-cloud chemistry opens pathway to the formation of oxalic acid in the marine atmosphere, Atmos. Environ., 37, 2423-2427, http://dx.doi.org/10.1016/S1352-2310(03)00136-5, 2003.

Weller, C., Tilgner, A., Bräuer, P., and Herrmann, H.: Modeling the Impact of Iron–Carboxylate Photochemistry on Radical Budget and Carboxylate Degradation in Cloud Droplets and Particles, Environmental Science & Technology, 48, 5652-5659, 10.1021/es4056643, 2014.

Wu, J., Bei, N., Hu, B., Liu, S., Wang, Y., Shen, Z., Li, X., Liu, L., Wang, R., Liu, Z., Cao, J., Tie, X., Molina, L. T., and Li, G.: Aerosol–photolysis interaction reduces particulate matter during wintertime haze events, P. Natl. Acad. Sci. USA, 117, 9755-9761, 10.1073/pnas.1916775117, 2020.

Xu, B., Zhang, G., Gustafsson, Ö., Kawamura, K., Li, J., Andersson, A., Bikkina, S., Kunwar, B., Pokhrel, A., Zhong, G., Zhao, S., Li, J., Huang, C., Cheng, Z., Zhu, S., Peng, P., and Sheng, G.: Large contribution of fossil-derived components to aqueous secondary organic aerosols in China, Nat. Commun., 13, 5115, 10.1038/s41467-022-32863-3, 2022.

Xu, K., Cui, K., Young, L.-H., Wang, Y.-F., Hsieh, Y.-K., Wan, S., and Zhang, J.: Air Quality Index, Indicatory Air Pollutants and Impact of COVID-19 Event on the Air Quality near Central China, Aerosol and Air Quality Research, 20, 1204-1221, 10.4209/aaqr.2020.04.0139, 2020.

Yu, J. Z., Huang, X.-F., Xu, J., and Hu, M.: When Aerosol Sulfate Goes Up, So Does Oxalate: Implication for the Formation Mechanisms of Oxalate, Environmental Science & Technology, 39, 128-133, 10.1021/es049559f, 2005.

Yu, Q., Chen, J., Cheng, S., Qin, W., Zhang, Y., Sun, Y., and Ahmad, M.: Seasonal variation of dicarboxylic acids in PM2.5 in Beijing: Implications for the formation and aging processes of secondary organic aerosols, Sci. Total Environ., 763, 142964, https://doi.org/10.1016/j.scitotenv.2020.142964, 2021.

Yu, Q., Chen, J., Qin, W., Cheng, S., Zhang, Y., Ahmad, M., and Ouyang, W.: Characteristics and secondary formation of water-soluble organic acids in PM1, PM2.5 and PM10 in Beijing during haze episodes, Sci. Total Environ., 669, 175-184, https://doi.org/10.1016/j.scitotenv.2019.03.131, 2019.

Zaveri, R. A., Easter, R. C., Singh, B., Wang, H., Lu, Z., Tilmes, S., Emmons, L. K., Vitt, F., Zhang, R., Liu, X., Ghan, S. J., and Rasch, P. J.: Development and Evaluation of Chemistry-Aerosol-Climate Model CAM5-Chem-MAM7-MOSAIC: Global Atmospheric Distribution and Radiative Effects of Nitrate Aerosol, Journal of Advances in Modeling Earth Systems, 13, e2020MS002346, https://doi.org/10.1029/2020MS002346, 2021.

Zhang, Y., Kawamura, K., Cao, F., and Lee, M.: Stable carbon isotopic compositions of low-molecular-weight dicarboxylic acids, oxocarboxylic acids, α-dicarbonyls, and fatty acids: Implications for atmospheric processing of organic aerosols, J. Geophys. Res. Atmos., 121, 3707-3717, 10.1002/2015jd024081, 2016.

Zhao, W., Kawamura, K., Yue, S., Wei, L., Ren, H., Yan, Y., Kang, M., Li, L., Ren, L., Lai, S., Li, J., Sun, Y., Wang, Z., and Fu, P.: Molecular distribution and compound-specific stable carbon isotopic composition of dicarboxylic acids, oxocarboxylic acids and α-dicarbonyls in $PM_{2.5}$ from Beijing, China, Atmos. Chem. Phys., 18, 2749-2767, 10.5194/acp-18-2749-2018, 2018.

Zhao, W., Ren, H., Kawamura, K., Du, H., Chen, X., Yue, S., Xie, Q., Wei, L., Li, P., Zeng, X., Kong, S., Sun, Y., Wang, Z., and Fu, P.: Vertical distribution of particle-phase dicarboxylic acids, oxoacids and α-dicarbonyls in the urban

boundary layer based on the 325 m tower in Beijing, Atmos. Chem. Phys., 20, 10331-10350, 10.5194/acp-20-10331-2020, 2020.

Zhao, X., Pavuluri, C. M., Dong, Z., Xu, Z., Nirmalkar, J., Jung, J., Fu, P., and Liu, C.-Q.: Molecular Distributions and 13C Isotopic Composition of Dicarboxylic Acids, Oxocarboxylic Acids, and α-dicarbonyls in Wintertime PM2.5 at Three Sites Over Northeast Asia: Implications for Origins and Long-Range Atmospheric Transport, Journal of Geophysical Research: Atmospheres, 128, e2023JD038864, https://doi.org/10.1029/2023JD038864, 2023.

Zhong, H., Huang, R., Chang, Y., Duan, J., Lin, C., and Chen, Y.: Enhanced formation of secondary organic aerosol from photochemical oxidation during the COVID-19 lockdown in a background site in Northwest China, Sci. Total Environ., 778, 144947, https://doi.org/10.1016/j.scitotenv.2021.144947, 2021.

Zhou, Y., Huang, X. H., Bian, Q., Griffith, S. M., Louie, P. K. K., and Yu, J. Z.: Sources and atmospheric processes impacting oxalate at a suburban coastal site in Hong Kong: Insights inferred from 1 year hourly measurements, Journal of Geophysical Research: Atmospheres, 120, 9772-9788, https://doi.org/10.1002/2015JD023531, 2015.

Table 1. Meteorological parameters, liquid water content (LWC) of aerosol, in-situ pH (pH_{is}), and chemical compositions of $PM_{2.5}$ before (January 6 – 23, 2020) and during the lockdown (LCD) (January 31 – February 17, 2020) in Jinan, China.

	Before the LCD (*n*=36)	During the LCD (*n*=36)	Whole period (*n*=72)
I. Meteorological parameters			
Temperature (°C)	0.07 ±5.9 (-16–13)	6.8 ±5.2 (-3.4–16)	3.4 ±6.5 (-16–16)
Relative humidity (%)	52 ±10 (30–87)	39 ±18 (17–85)	45 ±16 (17–87)
Solar radiation (W m^{-2})	164 ±70 (32–282)	255 ±117 (18–423)	209 ±106 (18–423)
Wind speed (m s^{-1})	3.0 ±0.7 (1.6–4.6)	3.7 ±1.1 (1.2–6.6)	3.3 ±1.0 (1.2–6.6)
II. Gaseous pollutants (μg m^{-3})			
SO_2	23 ±8.9 (8.3–49)	14 ±4.9 (4.9–29)	18 ±8.5 (4.9–49)
NO_2	56 ±12 (38–82)	21 ±5.9 (9.3–34)	38 ±20 (9.3–81)
CO	1.6 ±0.3 (0.9–2.5)	0.9 ±0.2 (0.5–1.6)	1.3 ±0.5 (0.5–2.5)
O_3	29 ±18 (5.3–74)	66 ±21 (25–109)	48 ±27 (5.3–109)
OH ·radicals (×10^6 cm^{-3})	9.7 ±9.1 (0.2–21)	14 ±15 (0.3–34)	12 ±12 (0.2–34)
Ⅲ. Inorganic ions (μg m^{-3})			
K^+	1.0 ±0.1 (0.9–1.7)	1.3 ±0.6 (0.5–2.9)	1.1 ±0.4 (0.5–2.9)
Na^+	0.3 ±0.1 (0.1–0.6)	0.2 ±0.1 (0.1–0.8)	0.2 ±0.1 (0.1–0.8)
Ca^{2+}	0.4 ±0.2 (0.1–0.9)	0.5 ±0.2 (0.2–1.1)	0.5 ±0.2 (0.1–1.1)
Mg^{2+}	0.1 ±0.03 (0–0.1)	0.1 ±0.1 (0.1–0.4)	0.1 ±0.1 (0–0.4)
NH_4^+	11 ±5.7 (4.4–26)	7.7 ±4.7 (0.4–16)	9.6 ±5.5 (0.4–26)
NO_3^-	19 ±11 (5.4–49)	9.6 ±4.9 (1.2–18)	14 ±9.7 (1.2–49)
SO_4^{2-}	13 ±6.9 (3.8–31)	9.4 ±5.3 (1.1–18)	11 ±6.4 (1.1–31)
SNA[a]	44 ±23 (15–105)	27 ±15 (2.8–50)	35 ±21 (2.8–105)
Subtotal	49 ±24 (18–113)	35 ±18 (6.1–67)	42 ±22 (6.1–113)
Ⅳ. Carbonaceous species (μg m^{-3})			
EC	4.3 ±2.4 (0.9–11)	1.9 ±1.0 (0.3–3.8)	3.1 ±2.2 (0.3–11)
OC	10 ±3.0 (5.2–19)	6.4 ±2.6 (2.0–11)	8.3 ±3.4 (2.0–19)
WSOC	3.9 ±1.9 (1.2–10)	3.2 ±1.4 (1.0–7.0)	3.5 ±1.7 (1.0–10)
OC/EC	2.9 ±1.3 (1.5–6.9)	4.0 ±1.5 (2.4–8.4)	3.5 ±1.5 (1.5–8.4)
WSOC/OC	0.4 ±0.1 (0.2–0.7)	0.5 ±0.1 (0.3–0.8)	0.4 ±0.1 (0.2–0.8)
Ⅴ. Other species			
$PM_{2.5}$ (μg m^{-3})	106 ±45 (35–202)	56 ±29 (10–111)	81 ±46 (10–202)
PM_{10} (μg m^{-3})	147 ±58 (38–285)	72 ±33 (19–129)	109 ±60 (19–285)
Levoglucosan (ng m^{-3})	141 ±70 (50–370)	102 ±29 (61–186)	121 ±57 (50–370)
pH_{is}	3.2 ±3.0 (2.3–7.7)	3.5 ±3.5(2.8–4.9)	3.3 ±3.1 (2.3–7.7)
LWC (μg m^{-3})	35 ±33 (4.3–172)	10 ±10 (0.2–45)	24 ±30 (0.2–172)
$SNA/PM_{2.5}$ (%)	40 ±6.5 (29–54)	47 ±8.2 (28–60)	43 ±8.1 (28–60)
N/S[b]	1.5 ±0.3 (0.9–2.4)	1.1 ±0.2 (0.7–1.5)	1.3 ±0.4 (0.7–2.4)

[a]Total concentration of SO_4^{2-}, NO_3^-, and NH_4^+.
[b]The ratio of NO_3^-/SO_4^{2-}.

885

Table 2. Concentrations (ng m^{-3}) of dicarboxylic acids, oxocarboxylic acids, and α-dicarbonyls in $PM_{2.5}$ before and during the LCD in Jinan, China.

Compounds	Before the LCD (n = 36)	During the LCD (n = 36)	Whole period (n = 72)
I. Dicarboxylic acids			
Oxalic, C_2	181 ±48 (110–381)	239 ±108 (46–478)	210 ±88 (46–478)
Malonic, C_3	15 ±4.3 (5.2–26)	45 ±14 (18–79)	30 ±19 (5.2–79)
Succinic, C_4	54 ±29 (15–178)	30 ±13 (11–66)	42 ±25 (11–178)
Glutaric, C_5	6.7 ±4.5 (0.6–20)	7.5 ±4.0 (0.7–15)	7.1 ±4.2 (0.6–20)
Adipic, C_6	9.2 ±8.6 (1.7–41)	6.1 ±3.3 (0.9–14)	7.6 ±6.7 (0.9–41)
Pimelic, C_7	2.3 ±1.5 (0.2–7.4)	1.9 ±1.4 (0–5.1)	2.1 ±1.5 (0–7.4)
Suberic, C_8	7.7 ±4.7 (1.9–23)	3.0 ±2.4 (0.1–13)	5.4 ±4.4 (0.1–23)
Azelaic, C_9	12 ±4.0 (5.8–24)	5.9 ±4.8 (0.4–23)	9.0 ±5.3 (0.4–24)
Sebacic, C_{10}	3.9 ±2.3 (1.3–9.9)	2.6 ±1.5 (0.2– 5.1)	3.3 ±2.0 (0.2– 9.9)
Undecanedioic, C_{11}	4.0 ±2.9 (0.5–15)	3.5 ±1.9 (0.3–8.6)	3.8 ±2.4 (0.3–15)
Methylmalonic, iC_4	3.5 ±4.1 (0.2–13)	4.8 ±4.6 (0–17)	4.1 ±4.4 (0–17)
Mehtylsuccinic, iC_5	4.2 ±3.5 (0.4–12)	3.4 ±1.6 (0.4–6.1)	3.8 ±2.7 (0.4–12)
Methyglutaric, iC_6	2.2 ±1.1 (0.4–5.6)	2.4 ±1.4 (0–6.6)	2.3 ±1.3 (0–6.6)
Maleic, M	6.9 ±6.2 (0.8–34)	5.0 ±2.3 (0.6–11.0)	5.9 ±4.7 (0.6–34)
Fumaric, F	10 ±7.6 (2.3–44)	1.5 ±0.9 (0.2–4.8)	5.8 ±6.9 (0.2–44)
Methylmaleic, mM	5.5 ±4.3 (1.4–22)	4.2 ±3.3 (0–16)	4.9 ±3.9 (0–22)
Phthalic, Ph	11 ±6.1 (2.9–34)	8.8 ±6.1 (1.2–25)	9.9 ±6.2 (1.2–34)
Isophthalic, iPh	3.0 ±3.9 (0.2–24)	1.8 ±2.4 (0–9.9)	2.4 ±3.3 (0–24)
Terephthalic, tPh	2.0 ±1.4 (0.2–7.5)	1.3 ±0.8 (0.1–2.6)	1.6 ±1.2 (0.1–7.5)
Ketomalonic, kC_3	2.1 ±1.4 (0.3–6.3)	3.0 ±1.7 (0.2–7.4)	2.6 ±1.6 (0.2–7.4)
Ketopimelic, kC_7	5.1 ±4.7 (0.8–20)	5.7 ±4.2 (0.2–17)	5.4 ±4.4 (0.2–20)
Subtotal	351 ±92 (212–672)	386 ±127 (121–707)	369 ±112 (121–707)
II. Oxocarboxylic acids			
Pyruvic, Pyr	13 ±4.9 (4.4–25)	21 ±8.8 (7.3–43)	17 ±8.2 (4.4–43)
Glyoxylic, ωC_2	24 ±9.1 (6.6–43)	29 ±8.5 (10–43)	26 ±9.0 (6.6–43)
3-Oxopropanoic, ωC_3	4.5 ±4.6 (0.8–25)	12 ±6.5 (0.6–27)	8.4 ±6.9 (0.6–27)
4-Oxobutanoic, ωC_4	7.1 ±6.4 (0.8–38)	3.1 ±2.7 (0–12)	5.1 ±5.3 (0–38)
7-Oxoheptanoic, ωC_7	2.3 ±2.2 (0.2–8.6)	1.9 ±2.0 (0–8.6)	2.1 ±2.1 (0–8.6)
8-Oxooctanoic, ωC_8	3.2 ±2.8 (0.4–16)	3.7 ±2.1 (0.1–9.3)	3.4 ±2.4 (0.1–16)
9-Oxononanoic, ωC_9	6.9 ±3.0 (1.5–15)	3.4 ±2.9 (0–9.0)	5.2 ±3.4 (0–15)
Subtotal	61 ±20 (25–106)	75 ±17 (37–104)	68 ±19 (25–106)
III. α-Dicarbonyls			
Glyoxal, Gly	13 ±6.3 (4.4–32)	13 ±5.3 (2.0–28)	13 ±5.8 (2.0–32)
Methylglyoxal, mGly	12 ±7.6 (2.6–30)	12 ±4.8 (2.4–21)	12 ±6.0 (2.4–30)
Subtotal	25 ±14 (7.8–62)	25 ±10 (4.4–49)	25 ±12 (4.4–62)
Total detected species	437 ±117 (246–833)	486 ±144 (179–825)	461 ±132 (179–833)

890 **Table 3. Differences in the stable carbon isotopic compositions ($\delta^{13}C$, ‰) of major detected diacids and related compounds before and during the LCD in Jinan, China.**

Compounds	Before the LCD (*n* = 36)	During the LCD (*n* = 36)	Whole period (*n* = 72)
	I. Dicarboxylic acids		
C_2	−22 ± 1.9 (−26 to −17)	−19 ± 2.5 (−24 to −14)	−20 ± 2.5 (−26 to −14)
C_3	−25 ± 4.2 (−36 to −19)	−23 ± 2.2 (−26 to −18)	−24 ± 3.6 (−36 to −18)
C_4	−28 ± 4.6 (−39 to −22)	−25 ± 2.4 (−29 to −20)	−26 ± 4.0 (−39 to −20)
C_6	−29 ± 3.4 (−38 to −23)	−27 ± 2.8 (−31 to −22)	−28 ± 3.3 (−38 to −22)
C_9	−27 ± 1.2 (−30 to −25)	−27 ± 2.3 (−32 to −24)	−27 ± 1.8 (−32 to −24)
Ph	−39 ± 6.4 (−51 to −27)	−30 ± 2.6 (−36 to −26)	−34 ± 6.4 (−51 to −26)
tPh	−37 ± 4.1 (−46 to −26)	−34 ± 0.9 (−36 to −32)	−35 ± 3.1 (−46 to −26)
	II. Oxocarboxylic acids		
Pyr	−28 ± 4.0 (−39 to −22)	−24 ± 2.3 (−29 to −20)	−26 ± 3.9 (−39 to −20)
ωC_2	−27 ± 3.6 (−38 to −22)	−23 ± 2.2 (−26 to −19)	−25 ± 3.6 (−38 to −19)
ωC_3	−29 ±4.0 (−40 to −24)	−26 ± 2.3 (−30 to −22)	−28 ± 3.7 (−40 to −22)
	III. α-Dicarbonyls		
Gly	−23 ± 3.7 (−36 to −19)	−20 ± 2.2 (−24 to −16)	−21 ± 3.5 (−36 to −16)
mGly	−25± 3.8 (−37 to −21)	−21 ± 2.0 (−25 to −18)	−23 ± 3.6 (−37 to −18)

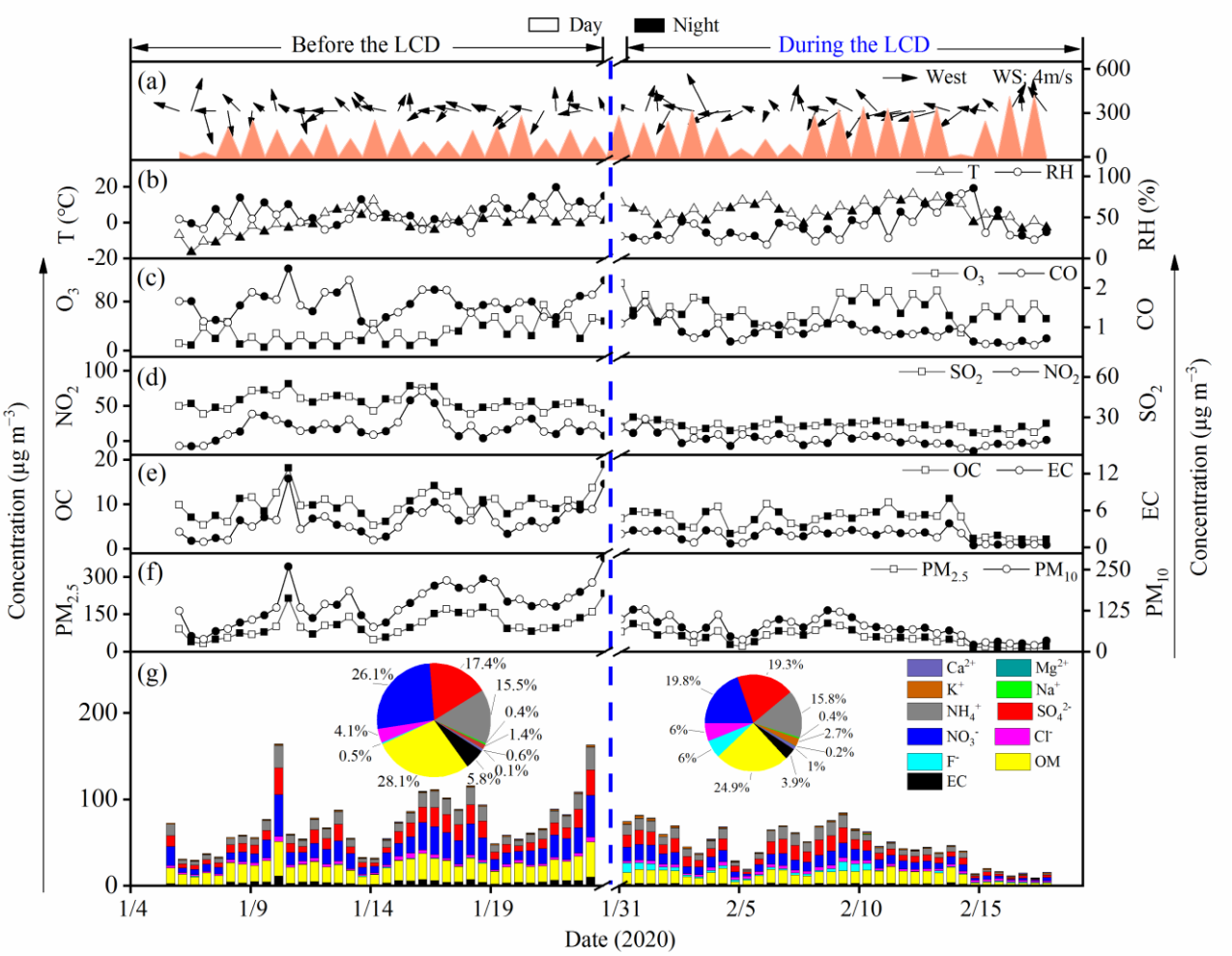

Figure 1. Temporal variations of gaseous pollutants, meteorological parameters, and chemical compositions of $PM_{2.5}$ before and during the LCD in Jinan, China.

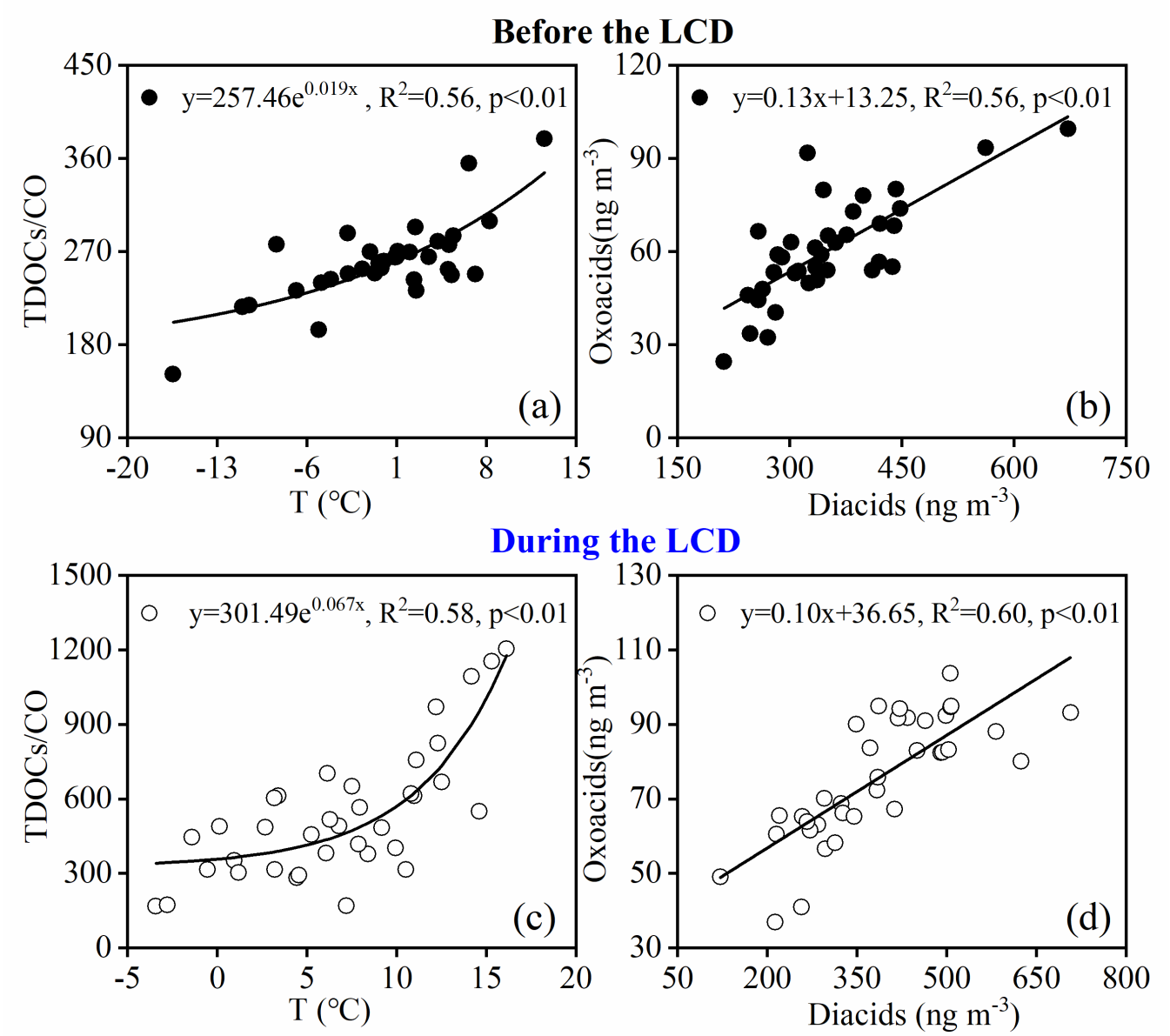

Figure 2. Correlation analysis between the ratio of the total concentration of detected organic components (TDOCs) normalized by CO (TDOCs/CO) and temperature, and between diacids and oxoacids (a) and (b) before the LCD, (c) and (d) during the LCD in Jinan, China.

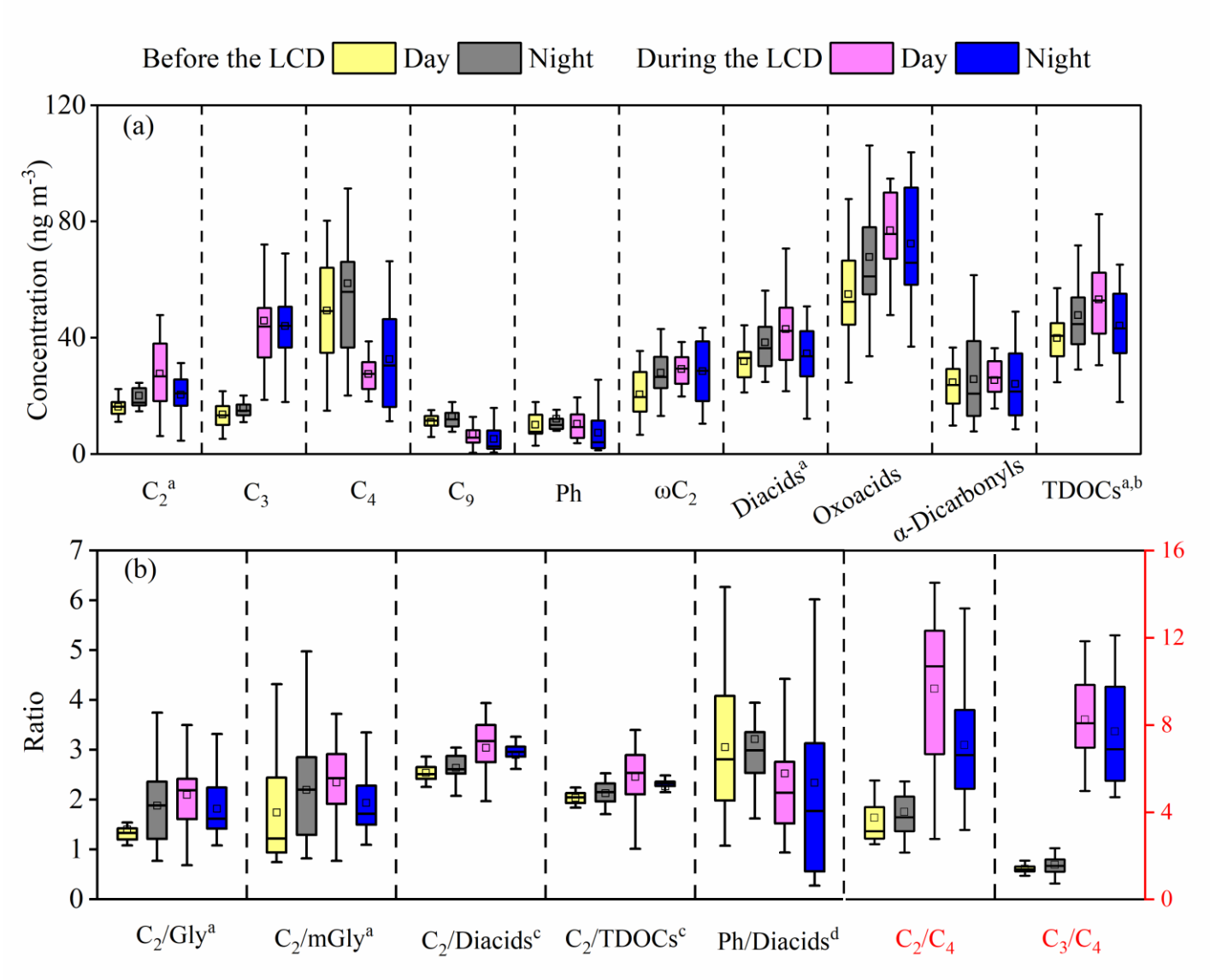

Figure 3. Diurnal changes of (a) major organic compounds and (b) selected mass ratios before and during the LCD in Jinan, China ([a] the concentrations reduced by 10 times; [b] TDOCs: total detected organic components; [c] the mass ratios enlarged by 5 times; [d] the mass ratio enlarged by 100 times).

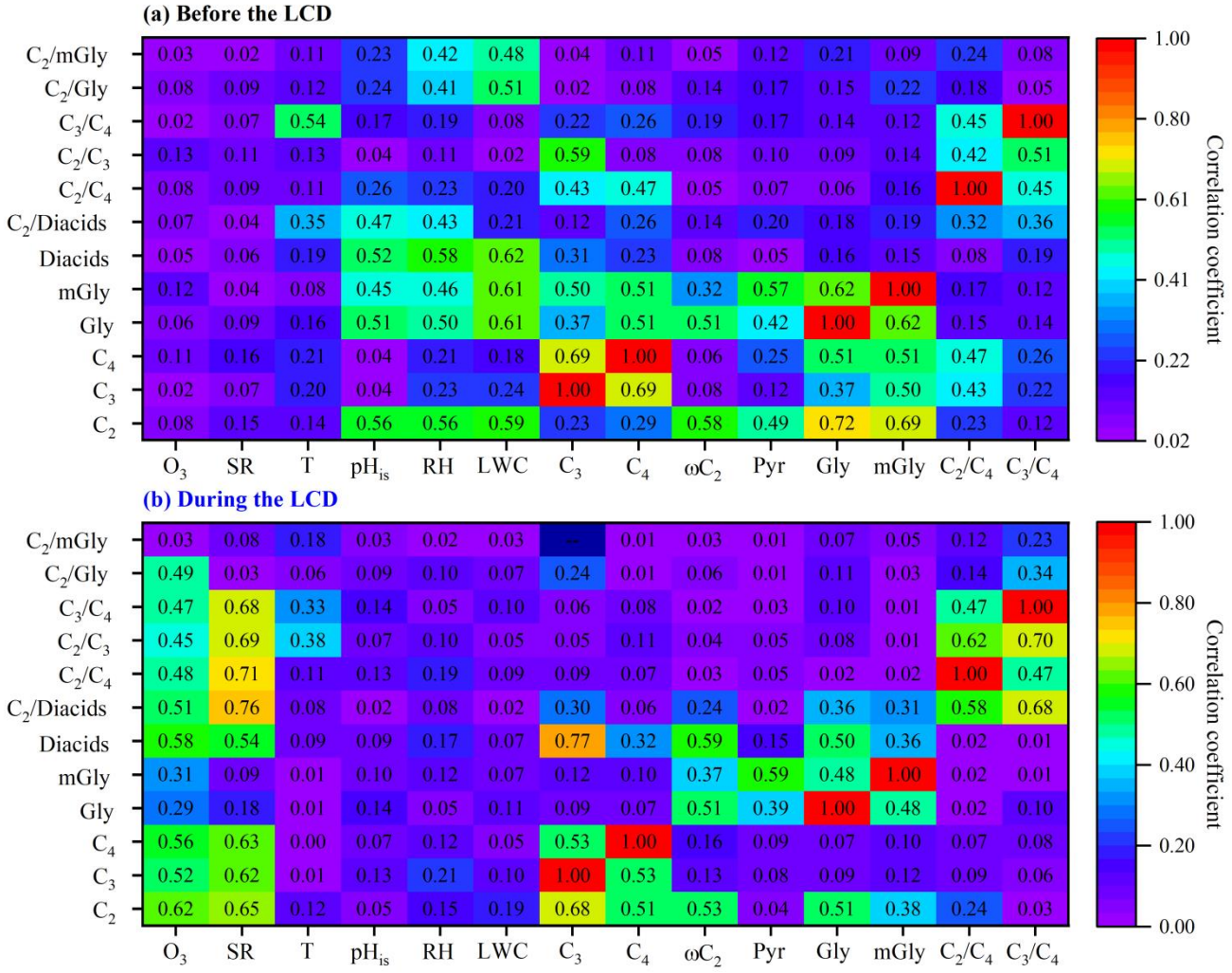

Figure 4. Correlation coefficients (R^2) of concentrations of C_2 and its organic precursors and selected ratios with influencing factors (a) before the LCD and (b) during the LCD in Jinan, China.

910

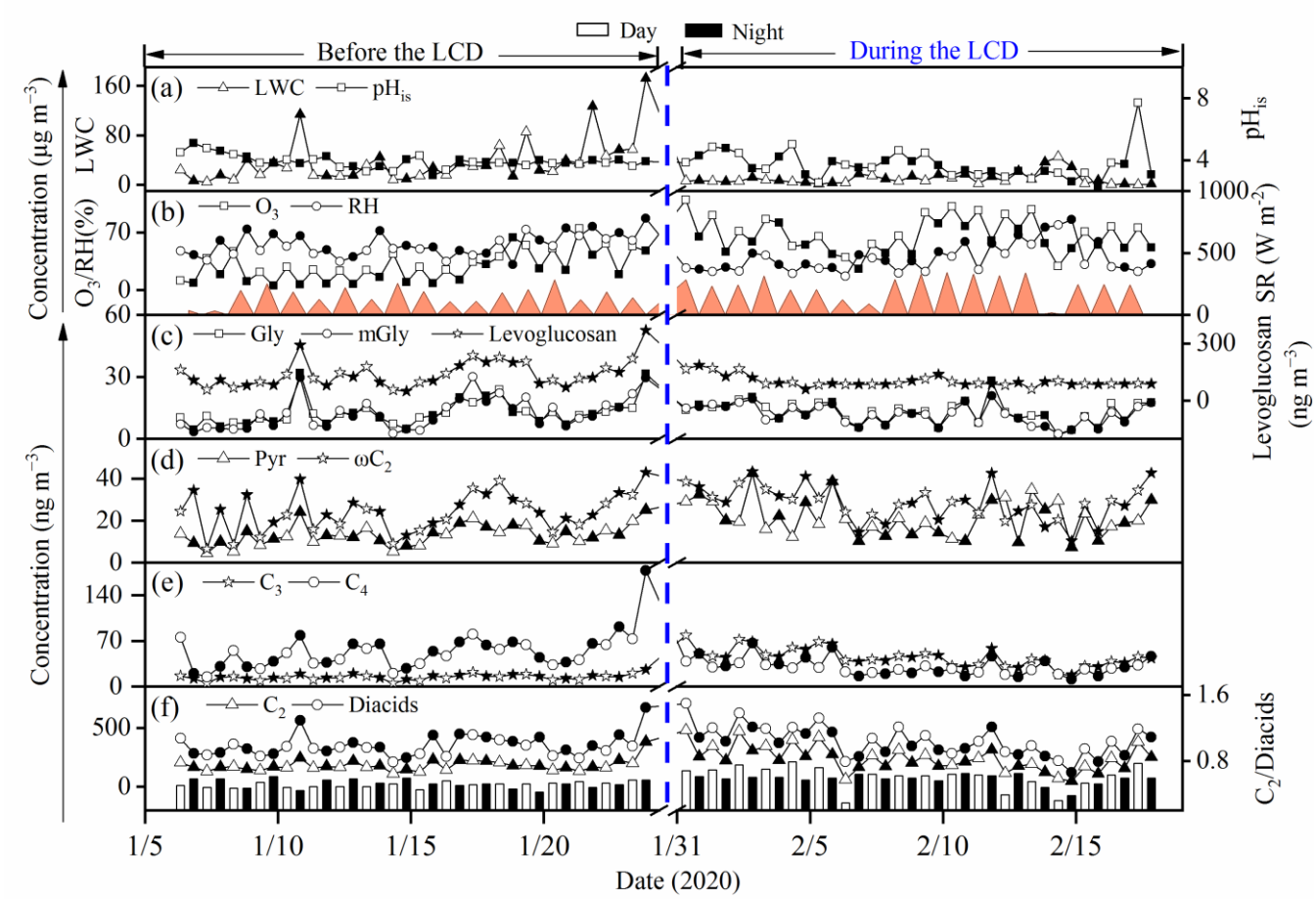

Figure 5. Temporal variations in the concentrations of levoglucosan, diacids, C_2 and its major precursors, the ratios of C_2/Diacids, as well as liquid water content (LWC), in-situ pH (pH_{is}), temperature, relative humidity (RH), solar radiation, and O_3 before and during the LCD in Jinan, China.

915

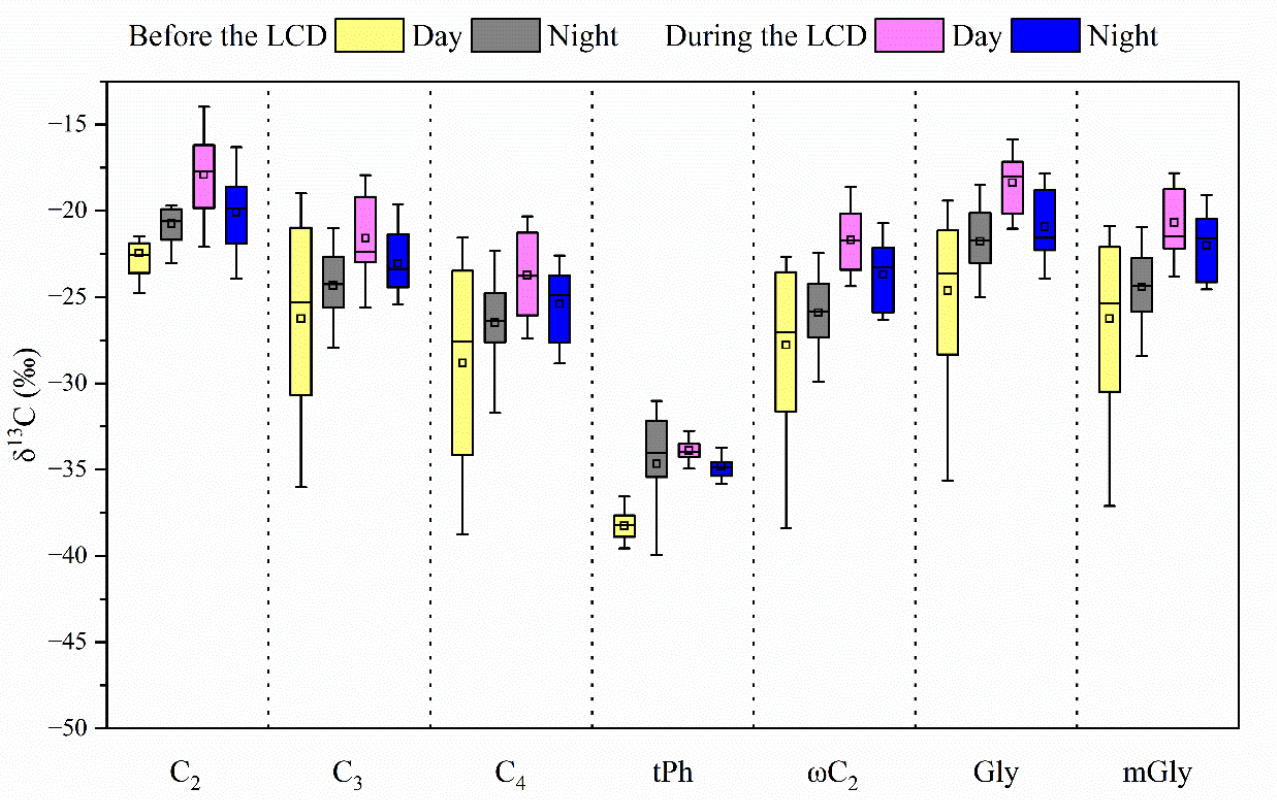

Figure 6. Differences in the stable carbon isotope compositions of major detected diacids (C_2–C_4, tPh), the smallest oxoacids (ωC_2), and α-dicarbonyls including Gly and mGly before and during the LCD in the atmosphere of Jinan, China.

920

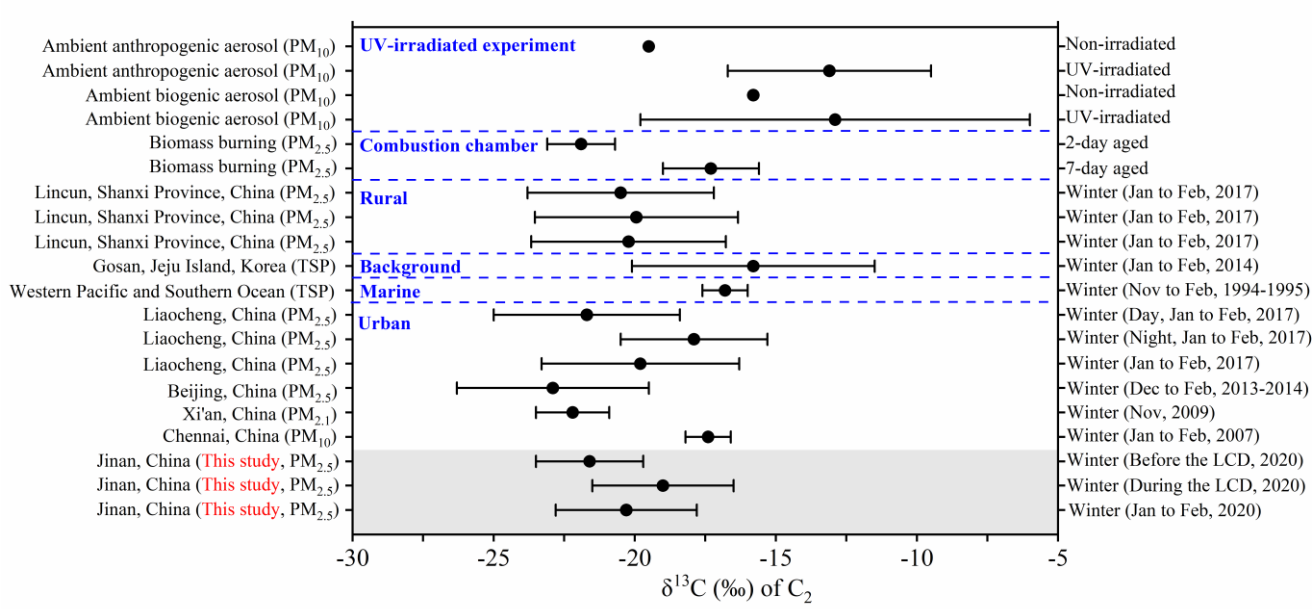

Figure 7. Comparison of stable carbon isotopic compositions ($\delta^{13}C$, ‰) of C_2 in aerosols of Jinan with those in other regions in the winter.

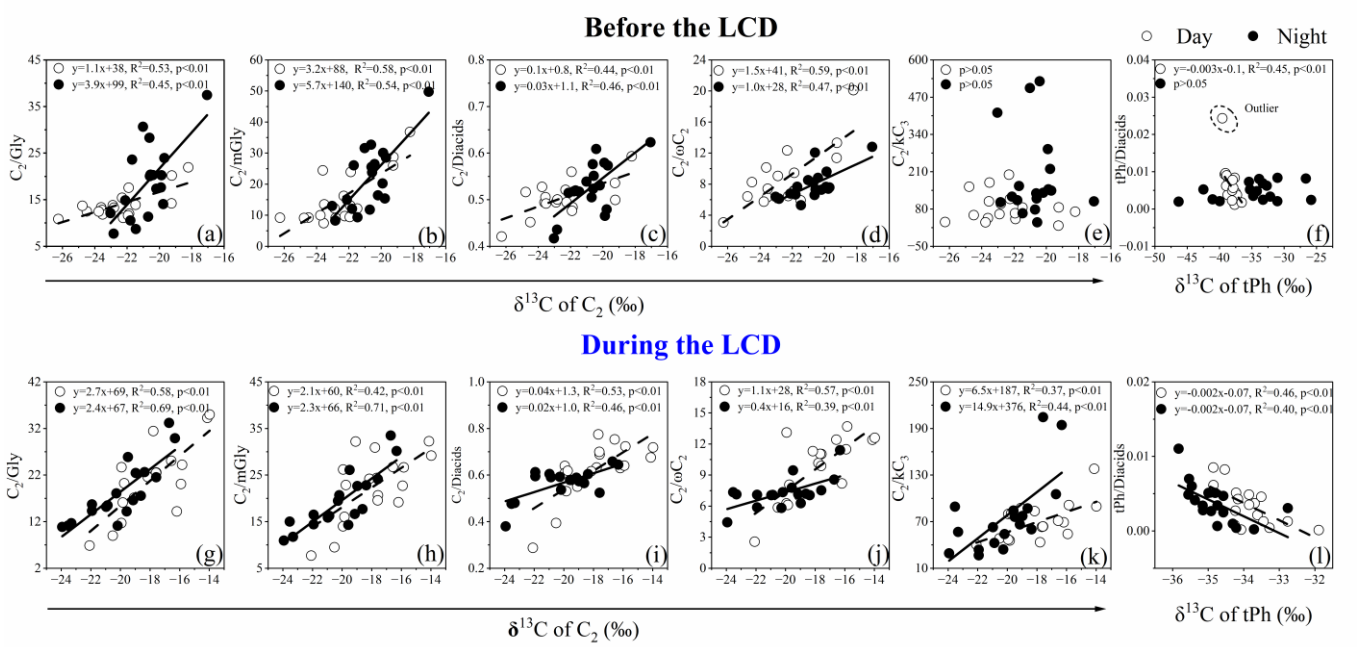

925

Figure 8. Correlations of the $\delta^{13}C$ of C_2 with the mass ratios of C_2/Gly, C_2/mGly, C_2/Diacids, $C_2/\omega C_2$, and C_2/kC_3, and the $\delta^{13}C$ of tPh with the mass ratio of tPh/Diacids before and during the LCD in January to February 2020.

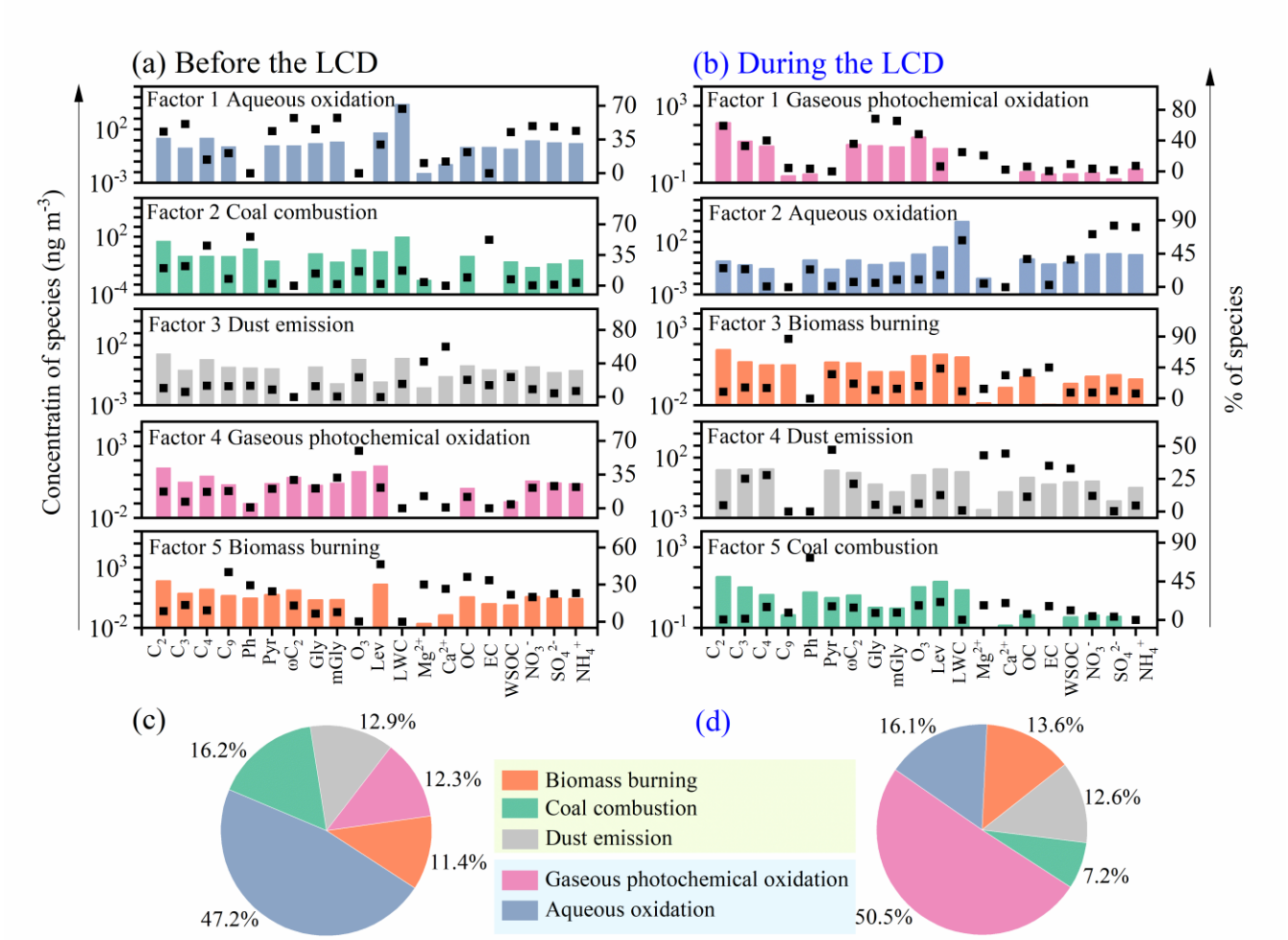

930 **Figure 9. Source profiles of major chemical components in the $PM_{2.5}$ samples from Jinan (a, c) before the LCD and (b, d) during the LCD (BB: biomass burning).**

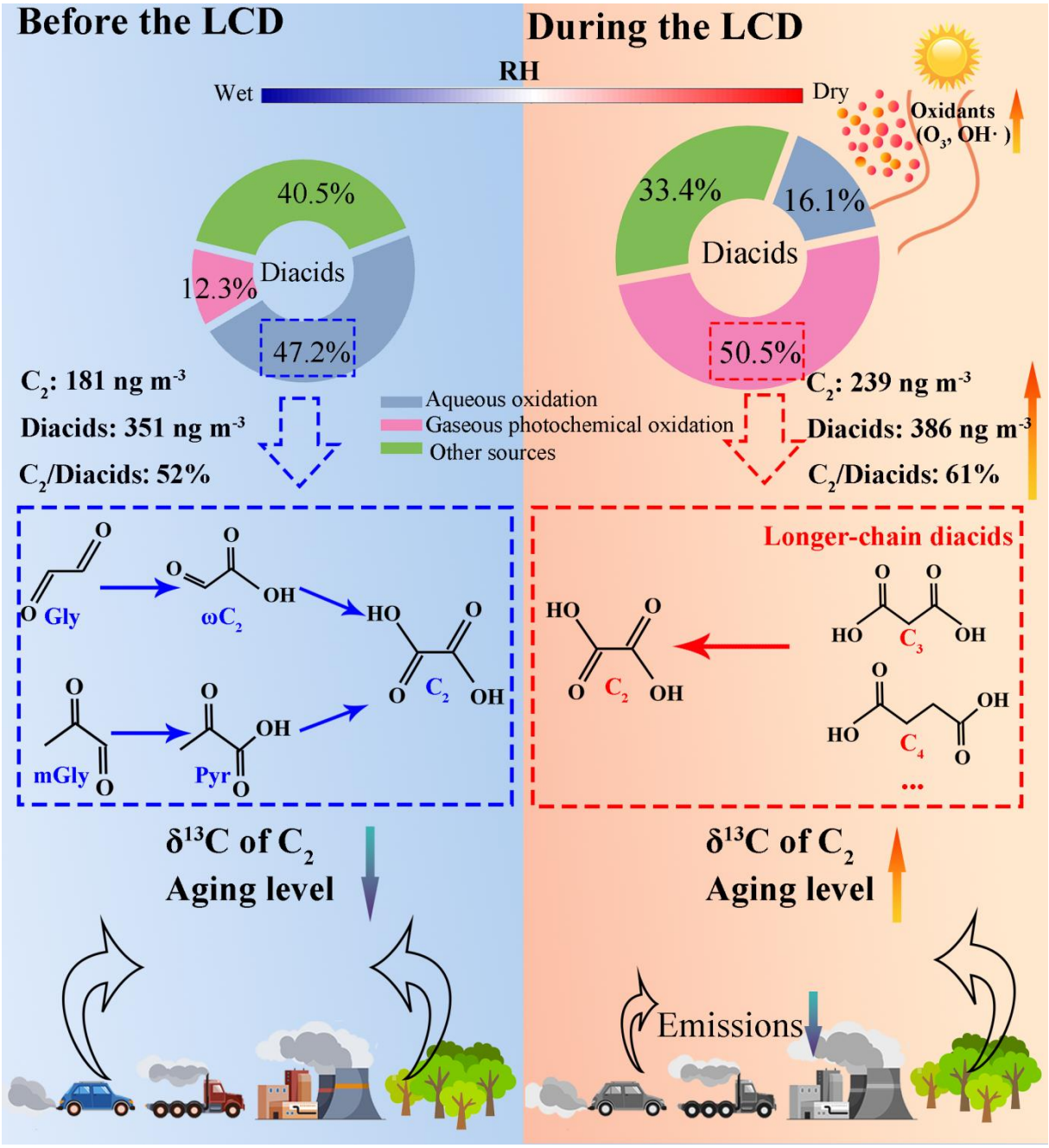

Figure 10. Schematic diagram illustrating the sources and formation mechanisms of C_2 and diacids before and during the LCD.

935